UPPSALA
UNIVERSITET

Digital Comprehensive Summaries of Uppsala Dissertations from the Faculty of Pharmacy 246

Mechanism-based modeling of biological processes involved in oral absorption

BENJAMIN GUIASTRENNEC

ACTA
UNIVERSITATIS
UPSALIENSIS
UPPSALA
2018

ISSN 1651-6192
ISBN 978-91-513-0225-6
urn:nbn:se:uu:diva-340238

Dissertation presented at Uppsala University to be publicly examined in A1:111a, Biomedicinskt centrum, Husargatan 3, Uppsala, Friday, 16 March 2018 at 09:15 for the degree of Doctor of Philosophy (Faculty of Pharmacy). The examination will be conducted in English. Faculty examiner: Dr Jörg Lippert (Clinical Pharmacometrics, Bayer AG, Leverkusen, Germany).

Abstract

Guiastrennec, B. 2018. Mechanism-based modeling of biological processes involved in oral absorption. *Digital Comprehensive Summaries of Uppsala Dissertations from the Faculty of Pharmacy* 246. 64 pp. Uppsala: Acta Universitatis Upsaliensis. ISBN 978-91-513-0225-6.

For orally administered drugs, the rate and extent of absorption are governed by the physiology of the gastrointestinal tract, the characteristics of the dosage form and the physico-chemical properties of the drug. This thesis primarily aimed to improve the mechanistic understanding and the predictability of processes involved in the absorption of orally administered drugs using a population modeling approach. A secondary aim was to propose an optimized dosing regimen for first line anti-tuberculosis drugs in underweight Indian children.

A model characterized the effect of pH, mechanical stress and formulation on *in vitro* extended release (ER) tablet erosion. The model was further used in combination with anatomical tablet location data to predict the *in vivo* erosion dynamics. The proposed approach could help address challenges related to the development of future ER formulations.

Gastric emptying regulates the rate of entry of nutrients into the small intestine. Bile acids are essential for the intestinal absorption of lipophilic drugs, but the determination of their local intestinal concentrations is difficult. A modeling framework was developed to characterize the relationships between nutritional intake, rate of gastric emptying, gallbladder emptying–refilling patterns and plasma concentrations of bile acids. This modeling framework could be used in combination with systems pharmacology models to predict the drug-drug interactions and food effects associated with gastric emptying, as well as to link the postprandial changes in plasma bile acid concentrations to the variability in drugs' absorption.

Optimal doses of first-line antituberculosis drugs have not been firmly established. In an underweight Indian children population, the pharmacokinetic-pharmacodynamic model identified rifampin as single predictor of unfavorable treatment outcome. Children with low body weight and/or HIV coinfection had a higher probability of unfavorable treatment outcome. Doses increase were proposed and could provide crucial information for future guidelines.

In summary, the developed models enabled the prediction of the *in vivo* erosion profile of ER formulations based on *in vitro* dissolution data. A modeling framework predicted the postprandial gastric emptying rate and enterohepatic circulation of bile acids. Finally, a model-based approach was used to identify risk factors and propose optimized dose recommendations in tuberculosis-infected Indian children.

Keywords: absorption, bile acids, enterohepatic circulation, food effect, gallbladder, in vitro in vivo correlation; NONMEM, pediatrics, pharmacometrics, tuberculosis

Benjamin Guiastrennec, Department of Pharmaceutical Biosciences, Box 591, Uppsala University, SE-75124 Uppsala, Sweden.

ISSN 1651-6192
ISBN 978-91-513-0225-6
urn:nbn:se:uu:diva-340238 (http://urn.kb.se/resolve?urn=urn:nbn:se:uu:diva-340238)

An expert is a person who has made all the mistakes that can be made in a very narrow field.

Niels Bohr

A ma famille

List of Papers

This thesis is based on the following papers, which are referred to in the text by their Roman numerals.

I **Guiastrennec B**, Söderlind E, Richardson S, Peric A, Bergstrand M. (2017) *In Vitro* and *In Vivo* Modeling of Hydroxypropyl Methylcellulose (HPMC) Matrix Tablet Erosion Under Fasting and Postprandial Status. *Pharm Res.*, 34:847–859.

II **Guiastrennec B**, Sonne DP, Hansen M, Bagger JI, Lund A, Rehfeld JF, Alskär O, Karlsson MO, Vilsbøll T, Knop FK, Bergstrand M. (2016) Mechanism-Based Modeling of Gastric Emptying Rate and Gallbladder Emptying in Response to Caloric Intake. *CPT Pharmacometrics Syst. Pharmacol*., 5:692–700.

III **Guiastrennec B**, Sonne DP, Bergstrand M, Vilsbøll T, Knop FK, Karlsson MO. Model-Based Prediction of Plasma Concentration and Enterohepatic Circulation of Total Bile Acids in Human. *[Submitted]*

IV **Guiastrennec B**, Ramachandran G, Karlsson MO, Kumar AKH, Bhavani PK, Gangadevi NP, Swaminathan S, Gupta A, Dooley KE, Savic RM. (2018) Suboptimal Antituberculosis Drug Concentrations and Outcomes in Small and HIV-Coinfected Children in India: Recommendations for Dose Modifications. *Clin. Pharmacol. Ther. [Epub ahead of print]*

Contents

Abbreviations

API	active pharmaceutical ingredient
AUC	area under the concentration-time curve
BCS	biopharmaceutical classification system
BOV	between occasion variability
BSV	between subject variability
BTV	between tablet variability
CAL_{USI}	caloric content in the upper small intestine
CCK	cholecystokinin
CCK_F	first CCK plasma peak
CCK_L	second CCK plasma peak
CMC	critical micellar concentration
COV	a covariate
CV	coefficient of variation
DCP	calcium hydrogen phosphate
$efat_{duod}$	fat equivalent amount in duodenum
E_H	hepatic extraction
EHC	enterohepatic circulation
EMA	European medicines agency
ER	extended release
FDA	food and drug administration
FOCE	first-order conditional estimation
GB_{refill}	postprandial gallbladder refilling function
GI	gastrointestinal
HIV	human immunodeficiency virus
HPMC	hydroxypropyl methylcellulose
$HPMC_{tablet}$	total amount of HPMC remaining in the tablet
INH	isoniazid
IVIVC	*in vitro–in vivo* correlation
K_A	absorption rate constant
K_G	gastric emptying rate constant
K_M	$HPMC_{tablet}$ for which the release rate is half of V_{MAX}
MMM	magnetic marker monitoring
NLME	nonlinear mixed-effects
OFV	objective function value
OGTT	oral glucose tolerance test
PBPK	physiologically-based PK

PD	pharmacodynamic
PK	pharmacokinetic
PRM	a model parameter
$P_{unfavorable}$	probability of unfavorable treatment outcome
PZA	pyrazinamide
$R_{GB,out}$	rate of gallbladder emptying
RIF	rifampin
RNTCP	revised national TB control programme
RSE	residual standard error
RUV	residual unexplained variability
SCM	stepwise covariate modeling
T2D	type 2 diabetic
TB	tuberculosis
TBA	total bile acids
USP2	United States pharmacopeia dissolution apparatus 2
V_{MAX}	maximal HPMC release rate
VPC	visual predictive check
WHO	world health organization

Introduction

The oral route is the most common way of administering drugs. Oral dosage forms are often preferred by the patients, for their convenient, non-invasive and economical aspects. They are also appreciated by the manufacturers for their flexibility which allows to modulate the rate, extent and site of release of the active pharmaceutical ingredient (API). However, this route also presents some drawbacks, for instance the absorption in the gastrointestinal (GI) tract can suffer from poor bioavailability and high variability.[1] These drawbacks are imputable to changes in the physiology of the GI tract, the characteristics of the dosage form and the physicochemical properties of the API.[2,3]

Numerous studies have been conducted in an attempt to characterize the different aspects of drug absorption. Physiological effects of bile acids concentration, pH, intestinal permeability, motility and metabolic activity have been identified.[1] Pathological factors such as tuberculosis (TB) infection or malnutrition can also impair these processes and modify the exposure to the treatment drugs.[4] Adding-on to the complexity, the quantification of the effect of these factors is challenged by their variability and the complex procedures required to obtain *in situ* samples from the different GI fluids.[5]

In parallel, considerable efforts have been made to characterize the effect of factors inherent to the dosage form and the API, thus making *in vitro* testing a cornerstone of drug development. Recent *in vitro* tests have been developed to mimic *in vivo* physicochemical conditions with the use of biorelevant dissolution media for fasting and postprandial statuses, but in most cases, those remain static representations of highly dynamic systems.[6]

Given the complexity of the GI tract, accurate *in vivo* predictions cannot solely rely on *in vitro* testing and new approaches are needed. Nonlinear mixed-effects (NLME) modeling has proven to be a powerful tool for integrating multi-dimensional information and describing dynamic processes while considering multiple levels and sources of variability.[7] NLME modeling approaches have many applications including the establishment of *in vitro-in vivo* correlations (IVIVC)[8], the description of complex physiological processes[9], and the evaluation of the efficacy of dosing recommendations in special populations[10].

Oral drug absorption

Physiology

The human GI tract implicates numerous organs working together to process food for proper nutrient absorption (*Figure 1*).[1,3] These processes are synchronized via different hormonal and neural pathways.[11] The physicochemical properties (e.g. secretions volume, pH, mechanical stress) are varying between different GI segments and between fasting and postprandial states.[1,3]

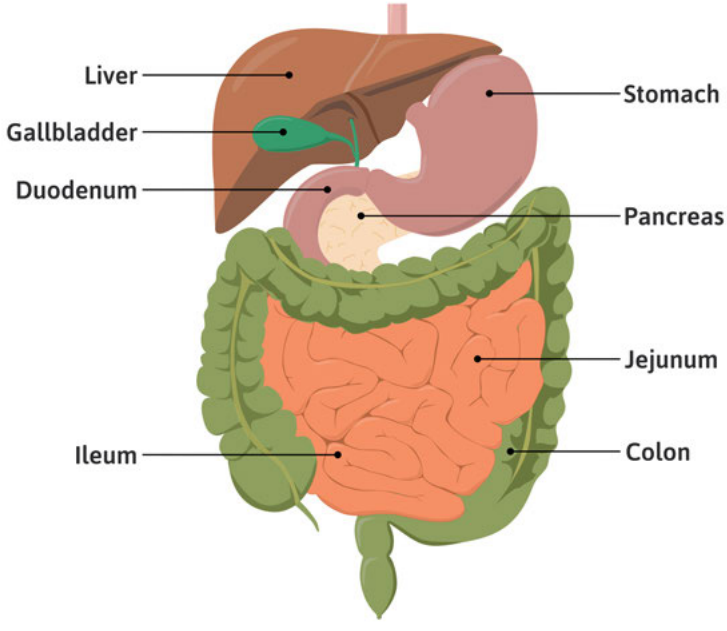

Figure 1. Schematic representation of the anatomy of the gastrointestinal tract.

In the fasting state the stomach has an acidic pH, relatively low volume of GI secretions and the migrating motor complex (i.e. strong peristaltic waves starting from the stomach and propagating through the small intestine) ensures the cleaning of the undigested matter.[1,12] In the postprandial state, the presence of food causes an increase in the stomach pH. The stomach acts as "gate keeper" of the small intestine. It holds, grinds and homogenizes the ingested food via the combined action of the walls' contraction and of the digestive enzymes. The transfer of the homogenized food or chyme from the stomach to the small intestine is called gastric emptying. The gastric emptying represents a key element of the GI tract, as it ensures a constant rate of caloric delivery and thus preventing the digestive and absorption processes in the small intestine from being overwhelmed.[13] The entry of the chyme into the small intestine, triggers the release of cholecystokinin (CCK), a gut hormone involved in the regulation of pancreatic enzyme secretion, intestinal motility, satiety signaling and

inhibition of gastric juice secretions.[14,15] This postprandial CCK elevation also triggers gallbladder contractions resulting in the flow of bile into the small intestine lumen.[11,15] The bile and pancreatic juices are mixed together with the chyme and propelled down the GI by the successive segmentation and peristaltic contractions phases of the small intestine. Along the small intestine, water and nutrients are gradually absorbed through the intestinal wall. The remaining unabsorbed material constitutes the faeces which are subsequently eliminated by the body via the colon.

Bile acids

Bile acids are water soluble, amphipathic molecules formed in the liver as an end product of cholesterol metabolism. These molecules are essential for the absorption of lipophilic compounds thanks to their emulsifying action. The total bile acids' (TBA) pool is mostly constituted of primary (cholic and chenodeoxycholic acids) and secondary (deoxycholic, ursodeoxycholic and lithocholic acids) bile acids that can be found in their glycine/taurine conjugate and unconjugated forms.[16,17] In the terminal part of the ileum, the primary bile acids are transformed into secondary bile acids and conjugated bile acids are deconjugated under the action of bacteria (*Figure 2*).[17]

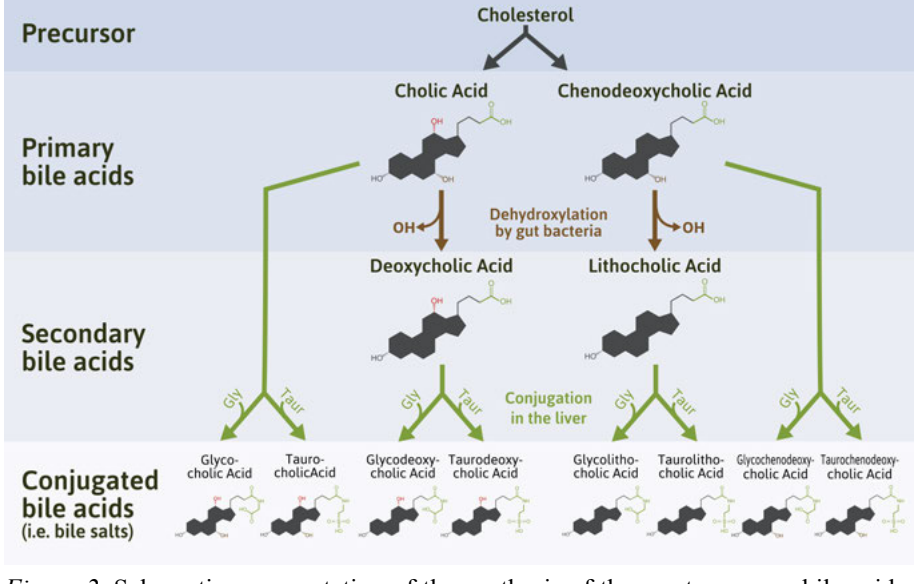

Figure 2. Schematic representation of the synthesis of the most common bile acids. Adapted from Mcstrother (Wikimedia Commons, licensed under CC BY 3.0).

In the fasting state, most of the bile flowing from the liver is directed toward the gallbladder, where it is stored and concentrated. Yet, about 10% of the incoming bile flows into the duodenum during this period.[18] When the chyme

enters the duodenum, the bile flow is directed toward the intestinal lumen by the coordinated relaxation of the Oddi sphincter and contractions of the gallbladder.[17,18] In the upper small intestine, about 30% of the bile acids (mainly unconjugated forms) are absorbed by passive diffusion.[19,20] The remaining fraction represented by ionized bile acids cannot cross the cell membranes and is thus propelled down the small intestine. Along the small intestine, the water is progressively being reabsorbed causing an increase in the concentration of bile acids. Above a certain threshold called the critical micellar concentration (CMC) the bile acids are forming micelles (i.e. aggregate of surfactant molecules in a colloidal solution). These micelles are essential to the emulsification of fat and lipophilic molecules (e.g. lipophilic vitamins and API).[16,21] Bile acids are efficiently (~95%) reabsorbed via active transporters in the terminal part of the ileum; the remaining 5% is excreted with the feces.[16] Upon their re-absorption, the bile acids transit through the portal vein to the liver where they are efficiently conjugated and extracted (55-90%). However, part of the bile acids escapes this hepatic extraction (E_H) and reaches the systemic circulation, this pool constitutes the "spillover".[17,22] The bile acids, extracted by the liver, are actively secreted into the biliary canaliculus, from which they either flow back directly to the small intestine or to the gallbladder.[17,18] This cycle is known as the enterohepatic circulation (EHC) of the bile acids and can occur several times during each meal (*Figure 3*).[17]

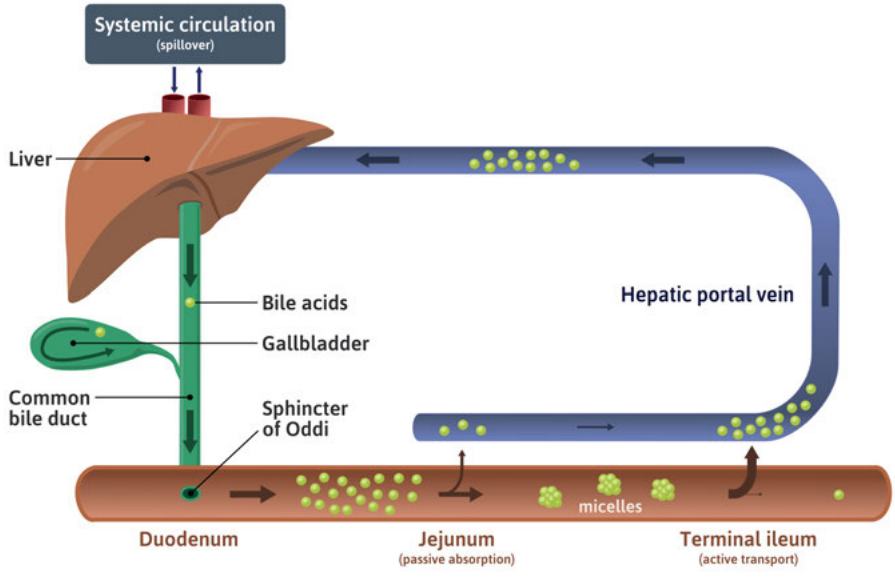

Figure 3. Schematic representation of the EHC of bile acids. Note, organs are not to scale.

In vitro–in vivo correlation

According to the United States pharmacopeia, an IVIVC is the ability to "find a relationship between an *in vitro* characteristic of a dosage form and its *in vivo* performance".[23] In other words, *in vitro* tests are used to predict the PK and PD characteristics in animal and human. IVIVC has a central role in the drug development process.[1] In fact, according to guidance from the European Medicines Agency (EMA)[24] and from the Food and Drug Administration (FDA)[25], some *in vivo* studies (e.g. bioequivalence studies) can be waived when a strong IVIVC can be demonstrated. Nevertheless, establishing strong IVIVC can be challenging for some API.[1,26]

The BCS classification

Amidon *et al.* established the biopharmaceutical classification system (BCS) in order to anticipate the IVIVC of API based on their aqueous solubility and GI permeability (*Table 1*). [2,27] The recent years have seen an increase in the number of lipophilic compounds entering development pipelines.[28] Lipophilic compounds labeled as BCS class II (i.e. high permeability) and IV (i.e. low permeability) often exhibit a low bioavailability in the fasting state. However, for some of these compounds, the bioavailability can be improved by the use of specific formulations or by the concomitant administration of a high-fat meal. This increased bioavailability is imputable to the inhibition of efflux transporters and to the solubilizing action of the bile acids micelles.[29,30] While the BCS classification can be used to anticipate the pharmacokinetic (PK) behavior and the effect of food for some of the classes, it does not allow to identify specific influential factors (e.g. meal properties), nor to quantify the variability and the magnitude of these effects on the PK parameters.[3,29,31]

Table 1. *BCS classification and meal effect for immediate release dosage forms*

Class	**Solubility**[a]	**Permeability**[b]	**Expected effect of a high-fat meal**[27,29]	**Relevant examples**
I	High	High	No effect on bioavailability, increased T_{MAX}	isoniazid[32 c]
II	Low	High	Increased bioavailability, variable effect on T_{MAX}	rifampin[33]
III	High	Low	Decreased bioavailability, increased T_{MAX}	acetaminophen[34], pyrazinamide[35] and isoniazid[32 c]
IV	Low	Low	Variable effects	–

T_{MAX}: time to plasma peak. [a] A high solubility is defined as the solubilization of a biorelevant dose of API in ≤250 mL of aqueous media (37°C and 1–7.5 pH); [b] A high permeability is defined as an extent of absorption ≥ 90% of the administered dose in human; [c] isoniazid is at the border between BCS class I and III.

ER formulations

Immediate release oral dosage forms start releasing the API as soon as they enter in contact with GI fluids. For some API this behavior may need to be modulated by using modified release formulations. This type of formulations can for example be used to reduce the GI-related toxicities, bypass the first-pass metabolism or enhance the solubility of lipophilic API. Common modified release formulation feature: extended release (ER), delayed release, targeted release and orally disintegrating dosage forms.[36] Herein, the focus is on the ER type dosage forms, commonly used to reduce the dosing frequency for API with short elimination half-life and to reduce the side effects of API exhibiting highly variable plasma concentrations. Hydrophilic matrices tablets are a common type of ER dosage forms where an API is dispersed through a hydrophilic polymer such as hydroxypropyl methylcellulose (HPMC). HPMC is known for its a safe and biodegradable profile, its compatibility with numerous API and its high load capacity. When ingested, the HPMC matrix swells and forms a rubbery gel caused by the diffusion of water into the tablet glassy core. Hydrophilic API are released by their diffusion through the gel layer and into the dissolution media, while the less soluble API and the HPMC polymer itself are released via the progressive erosion of the gel layer (*Figure 4*).[37–40] The proportion of HPMC within the tablet and its different properties can be adjusted to modulate the release rate of an API to specific therapeutic needs.[41] The development of HPMC matrix tablets can be challenging due to the numerous factors influencing their rate of erosion and hence requires extensive *in vitro* testing to achieve the desired release profile.[37,38]

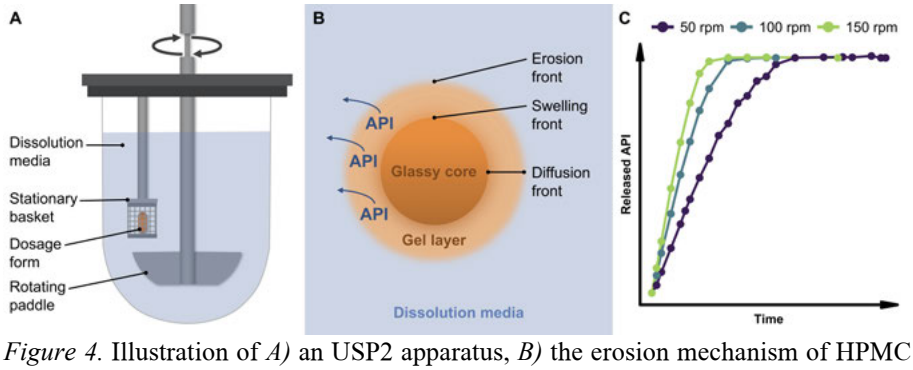

Figure 4. Illustration of *A)* an USP2 apparatus, *B)* the erosion mechanism of HPMC matrix tablets and *C)* the typical erosion time-course of HPMC matrix tablets.

In vitro dissolution testing

The development of oral dosage forms heavily relies on *in vitro* dissolution testing. The United States pharmacopeia dissolution apparatus 2 (USP2) is a widely used test developed to evaluate the erosion of tablets and the solubility

properties of an API over time (*Figure 4*). The USP2 experiments are typically conducted under a range of experimental conditions (e.g. pH, ionic strength and mechanical stress) to characterize the effect of covariates on the release rate (*Figure 4*).[42,43] The USP2 apparatus can also be used with biorelevant media (i.e. mimic the composition and properties of GI fluids) in order for example to evaluate the food effect on BSC class II compounds.[43] The use of the USP2 apparatus is however constrained to static *in vitro* experiments (i.e. fixed experimental conditions), though increasingly complex tests have recently been described.[42,44]

In vivo measurements

In vivo measurements provide essential information about different physiological and pharmacological factors in real conditions. They are used to confirm or infirm the predictions made by *in vitro* models and to improve the knowledge of the physiological and pathological processes. Trials in animals and humans are highly regulated and must comply with ethical guidelines to ensure that the burden to the subjects is minimal. Imaging techniques and biomarkers can give access to different variables while minimizing the costs and burden to the subjects (e.g. circumvent invasive sampling technique).

Tablet location and erosion rate

Magnetic marker monitoring (MMM) is a non-invasive, high resolution technique relying on the measurement of the magnetic dipole generated by labeled dosage forms using sensitive magnetic field sensors. The magnetic moment is generated by adding black iron oxide, a commonly used as food colorant, to the formulation and magnetizing it. This procedure allows for real-time *in vivo* monitoring of the erosion and the GI location of solid dosage forms under different prandial statuses.[9,45,46]

Gastric emptying rate

A direct measure of the gastric emptying rate would be a challenging task. Instead the plasma concentration of acetaminophen (i.e. paracetamol) following an oral dose can be used as surrogate. Acetaminophen, a BCS class III, is not absorbed through the stomach wall, but is extensively and rapidly absorbed in the upper small intestine.[29,47] Consequently, gastric emptying is the rate-limiting step in the absorption of acetaminophen and is therefore represented by the rate of appearance of acetaminophen in the systemic circulation.[48,49]

Bile acids distribution

Bile acids are naturally present in plasma making it challenging to evaluate some of their properties, such as their half-life in plasma. Among other, one

technique consists to administer of radiolabeled bile acids and to study their PK properties.[50]

TB in Indian children

TB is an infectious disease caused by the bacteria *mycobacterium tuberculosis* that generally affects the lungs. The infection occurs upon inhalation of infected droplets which are propelled into the air by the coughs, spits or sneezes of the infected subjects.[51]

Epidemiology and challenges

The World Health Organization (WHO) estimates that in 2016 about 718,000 children were newly infected and 253,000 deaths were caused by TB.[52] India bears the highest pediatric TB burden in the world, accounting for approximately 31% of all new cases.[52] Coinfection by the human immunodeficiency virus (HIV), young age and malnutrition are commonly encountered in TB-infected subjects in India. These aggravating factors can deteriorate the prognostic of the TB infection due to the intensification of the symptoms and a decreased exposure to treatment.[53,54] The assessment of the response to anti-TB treatment is challenging and consequently only a few studies have attempted to establish the exposure-response relationship of anti-TB drug in children.[55–58] Therefore, dosing recommendations for children are often based on adult data.[59]

RNTCP treatment guidelines

The treatment of drug sensitive TB typically starts with a 2-month intensive phase comprising of treatment by isoniazid (INH), rifampin (RIF), pyrazinamide (PZA) and ethambutol, followed by a 4-month continuation phase of treatment by INH and RIF.[4]

In India, the Revised National TB Control Programme (RNTCP), created in 1997 to reduce the incidence of TB by providing the diagnosis and the full treatment course for free and by using the directly observed treatment short-course strategy to ensure high levels of adherence.[60] However, the thrice-weekly dosing of first line anti-TB treatment previously recommended by the RNTCP (*Table 2*) has been shown to lead to suboptimal anti-TB drug concentrations in adults and children.[61,62] Thus, in 2012 the RNTCP pediatric guidelines were revised, to increase the RIF dose from 10 to 15 mg/kg and to refine the treatment weight bands, nevertheless the thrice-weekly dosing was kept.[63] More recently in 2016, the RNTCP pediatric guidelines were revised one more time to finally adopt a once-daily dosing regimen and fixed dose combination tablets in an effort to align with the recommendations from the WHO (*Table*

2).[64,65] These new guidelines were however not officially launched until November 2017.[66] In this thesis work, the pre-2012 and 2016 guidelines will respectively be referred to as the "previous" and the "new" RNTCP guidelines.

Table 2. *Intensive phase pediatric treatment as recommended by the RNTCP*

Weight band	**Isoniazid dose**	**Rifampin dose**	**Pyrazinamide dose**	**Ethambutol dose**
kg	mg (mg/kg)[a]	mg (mg/kg)[a]	mg (mg/kg)[a]	mg (mg/kg)[a]
Previous thrice-weekly RNTCP recommendations[b] [63]				
6–10	75 (9.4)	75 (9.4)	250 (31.3)	200 (25.0)
11–17	150 (10.7)	150 (10.7)	500 (35.7)	400 (28.6)
18–25	225 (10.5)	225 (10.5)	750 (34.9)	600 (27.9)
26–30	300 (10.7)	300 (10.7)	1,000 (35.7)	800 (28.6)
New once-daily RNTCP recommendations[c] [65]				
4–7	50 (9.1)	75 (13.6)	150 (27.3)	100 (18.2)
8–11	100 (10.5)	150 (15.8)	300 (31.6)	200 (21.1)
12–15	150 (11.1)	225 (16.7)	450 (33.3)	300 (22.2)
16–24	200 (10.0)	300 (15.0)	600 (30.0)	400 (20.0)
25–29	225 (8.3)	375 (13.9)	850 (31.5)	575 (21.3)
30–39	250 (7.2)	450 (13.0)	1,100 (31.9)	750 (21.7)

[a] Doses in mg/kg are reported for the average body weight of each weight band; [b] Doses administered thrice-weekly using single drug formulation tablets; [c] Doses administered once-daily using fixed dose combination tablets.

Pharmacometrics

Context and definition

In 2013, bringing a new drug to the market had an estimated average cost of 2.5 billion dollars, a number that has almost doubled through the last decade.[67] Facing this situation, the FDA launched in 2004 the Critical Path Initiative to in an effort to modernize the drug development process by incorporating the most recent scientific advances. In the associated white paper, the FDA stated:

> "A new product development toolkit — containing powerful new scientific and technical methods such as animal or computer-based predictive models, biomarkers for safety and effectiveness, and new clinical evaluation techniques — is urgently needed to improve predictability and efficiency along the critical path from laboratory concept to commercial product."[68]

Pharmacometrics is defined as "the science of developing and applying mathematical and statistical methods to characterize, understand, and predict a drug's PK, pharmacodynamic (PD), and biomarker-outcomes behavior"[69].

Through the last decade, this emerging science has been gaining consideration, and will likely continue to do so according to the *Pharmacometrics 2020 strategic goals* issued by the FDA.[70]

NLME models

NLME models are a central part of pharmacometrics. These models are used to describe a system of interest with a set of mathematical equations, typically implemented as ordinary differential equations. The term mixed-effects originates from the fact that the typical population parameters (i.e. fixed effects) and the variability (i.e. random effects) are modelled simultaneously. Different levels of variability can be modeled, including the variability between individuals, between occasions and the residual unexplained variability (RUV). Part of the variability, can be explained by the inclusion of covariate (e.g. tablet formulation, subject characteristics, etc.) on the different model parameters. The general form of an NLME model for continuous data can written as shown in *Equation 1*.

$$y_{ij} = f(t_{ij}, \theta, X_i, \eta_i) + \epsilon_{ij} \qquad \text{(Eq. 1)}$$

where y_{ij} is the dependent variable at the j^{th} observation of the i^{th} individual, $f(.)$ is a function of t_{ij} the independent variable, θ the vector of typical parameter values, X_i the matrix of covariates and η_i the vector of individual specific random effect parameters. η_i is assumed to follow a normal distribution of mean 0 and variance ω^2. The RUV represented by ε_{ij} is assumed to follow a normal distribution of mean 0 and variance σ^2. Of note, the RUV in *Equation 1* was implemented as an additive term, but several alternative implementations can also be used (e.g. proportional, combined).[69]

Maximum likelihood estimation methods

The maximum likelihood estimation is used to find the parameters that for a given model maximizes the likelihood of observing the data. For nonlinear models, the likelihood cannot be obtained directly and has to be approximated. Different approximation methods are available. In this work, the first-order conditional estimation (FOCE), and the Laplacian (second order) method will be used. The parameter estimation criterion relies on the minimization of the -2 log-likelihood called the objective function value (OFV) which is numerically easier than maximizing the likelihood.

Models for drug absorption

Depending on their complexity, PK models can be categorized from simple empirical models, more advanced mechanism-based models or highly complex physiologically-based PK (PBPK) models. The choice of developing/using either of these three categories is based on the purpose of the model and of the availability of data.

Empirical models

Empirical models are the most commonly developed models. With regards to absorption they can provide information such as the relative bioavailability, the delay and the absorption rate of an API.[71] However, the extrapolation to different populations or experimental conditions can be limited (e.g. prediction of the food effect on the absorption profile of a drug).

Mechanism-based models

Mechanism-based models are more complex and attempt to describe physiological and pharmacological processes as accurately as possible.[8,9] These models can to some extent be used to extrapolate outside the studied population or experimental conditions (e.g. a gastric emptying model can be used to predict the absorption profile of a drug under fasting and fed conditions). However, the development of mechanism-based models can be time consuming and lead to complex systems where not all parameters can be properly estimated. When the data (usually from several experiments) contains limited information to support the parameter estimation, frequentist priors can be introduced to stabilize the estimation step.[72] Alternatively, if no information in the data would allow adequate estimation of a specific parameter, it may be fixed to appropriate literature values and further evaluated through a sensitivity analysis.[10]

PBPK models

PBPK are extremely complex models, where parameters have been determined *a priori* based on *in vitro* and *in vivo* experiments. Due to their complexity these models are usually used for simulation only, although specific parameters can sometimes be estimated when sufficient data is available.[73] The main advantage of PBPK models is that they can be used to predict the PK of an API for which very limited information is available (i.e. early stage of drug development).[74] For example, the Advanced Dissolution, Absorption and Metabolism (ADAM) or the Advanced Compartmental Absorption and Transit (ACAT) models respectively developed by Simcyp® and GastroPlus™ can be used to predict the solubility, the precipitation, the GI transit and the membrane permeability of different API based on their physicochemical properties and the characteristics of the target population.[75,76]

Aims

The primary aim of this thesis was to improve the mechanistic understanding and the predictability of processes involved in the absorption of orally administered drugs through a NLME modeling approach. The secondary aim was to propose an optimized dosing regimen for the first line anti-TB drugs in underweight Indian children with and without concomitant HIV infection.

The specific aims were:

- To establish a model-based approach linking *in vitro* dissolution assays to *in vivo* erosion of ER solid dosage forms.

- To predict the relationship between the nutritional intake, the regulation of gastric emptying, gallbladder emptying and the spillover of bile acids in plasma.

- To propose an optimized dosing regimen for anti-TB therapy, with INH, RIF, PZA and ethambutol, in underweight Indian children with and without concomitant HIV infection.

Methods

All studies for which clinical data were included in this thesis were conducted in accordance with the good clinical practice standards. Ethical approval was obtained from appropriate local authorities and informed consent was obtained from all subjects. In *Paper IV* the data were obtained from two noninterventional studies where the subjects' parent/guardian provided a written informed consent; children aged 7 or older provided their assent.

Model development and evaluation

Software

Data were analyzed using a NLME modeling approach as implemented in the NONMEM software (v.7.3) and aided by functionalities of the PsN toolkit (v.4.4.2 or above).[77] The FOCE method with eta–epsilon interaction was used for continuous data and the Laplacian estimation method for discreet data. Data management, post-processing and model diagnostics were conducted in R (v.3.2.0 or above) and facilitated by functionalities of the package xpose (v.0.4.0 or above).[78]

Model selection and evaluation

Model selection was based on differences in the OFV, with a significance level of 5% for nested models. Graphical diagnostics, scientific plausibility and parameter uncertainty were also considered for model selection. Parameter uncertainty, which was reported as relative standard error (RSE) was obtained from the NONMEM sandwich estimator computed following an importance–sampling step.

Throughout their development, the predictive performances of the models were evaluated with visual predictive checks (VPC). In VPC, the 5^{th}, 50^{th} and 95^{th} percentiles of the observed data are compared to the 95% confidence interval around the 5^{th}, 50^{th} and 95^{th} percentiles of the simulated (n = 1,000) data.[79] In *Paper I*, prediction-corrected VPC were also used to evaluate the model performances across all experimental conditions and formulations simultaneously.[79]

Stochastic models

The variability in model parameters was evaluated at different levels. For *Paper I*, between tablet variability (BTV) was evaluated on the *in vitro* data, while between subject variability (BSV) and between occasion variability (BOV) were evaluated on the *in vivo* data. Each occasion was defined by the intake of a new formulation or a different prandial status. In *Paper II* and *Paper III,* the parameter variability was expressed as a single term accounting for both BSV and BOV. In *Paper IV* only BSV was evaluated.

For model parameters bound between 0 and 1, a logit transformation was applied prior to the implementation of the variability.[80] Log-normal distributions were used for parameters in the normal domain and normal distributions for parameters in the logit domain. In *Paper III* and *Paper IV*, correlations between parameters at the individual level were also evaluated.

Proportional, additive, and combined models were tested for the RUV on continuous data.

Covariate analysis

For *Paper II* to *Paper IV,* weight-based allometric scaling was applied to all volume and clearance parameters of the base models using exponents of 1 and ¾ respectively. The reference body weight was set to 70 kg for *Paper II* and *Paper III* and to 17.8 kg for *Paper IV*.[81]

For all papers, the covariate selection was performed through a stepwise covariate modeling (SCM) approach with forward inclusion ($P < 0.05$) and backward deletion ($P \geq 0.01$) steps. Categorical covariates were implemented as fractional change in the typical parameter value in relation to the most common category. Continuous covariates were first implemented linearly as fractional change in the typical parameter value for each unit change in the covariate to its median value (*Equation 2*); nonlinear relationships were only considered once covariates were included in the forward selection step.

$$PRM = TV_{PRM} \cdot (1 + S_{COV} \cdot (COV - COV_{MED})) \quad \text{(Eq. 2)}$$

where TV_{PRM} is the estimated typical value of the model parameter (PRM), S_{COV} is effect slope of the covariate (COV) on TV_{PRM} and COV_{MED} is the median value of COV.

In vitro–in vivo modeling of ER formulations

In vitro tablet erosion

Tablet erosion experiment data

The erosion of four HPMC-based ER formulations (*Table 3*) was investigated with an USP2 apparatus under a range of experimental conditions, namely mechanical stress (i.e. rotation speed), pH and ionic strength (*Table 4*).

Table 3. *Formulation of the HPMC-based ER tablets*[82]

Component	Formulation			
	no. 1	no. 2	no. 3	no. 4
Methocel K4M % (w/w)	23.0	10.0	-	-
Methocel K100LV % (w/w)	17.0	30.0	40.0	20.0
Calcium hydrogen phosphate % (w/w)	57.6	57.6	57.6	77.6
Black iron oxide % (w/w)	1.4	1.4	1.4	1.4
Sodium stearyl fumarate % (w/w)	1.0	1.0	1.0	1.0

Table 4. *Summary of the in vitro USP2 apparatus experimental conditions*

	pH 1.2		pH 6.8	
	Formulation	Mechanical stress (rpm)	Formulation	Mechanical stress (rpm)
Low ionic strength (98 mOsm/kg)	no. 1	-	no. 1	50/100/150
	no. 2	-	no. 2	25/50
	no. 3	-	no. 3	25/50/100/150
	no. 4	-	no. 4	50/100
High ionic strength (232 mOsm/kg)	no. 1	25/50/150	no. 1	50
	no. 2	50/100	no. 2	50
	no. 3	25/50/150	no. 3	50
	no. 4	50	no. 4	-

In vitro model development

An *in silico* tablet erosion model was developed to characterize the *in vitro* release of HPMC. A Michaelis-Menten type model (*Equation 3*) was pre-selected for its potential ability to describe changes in the tablet erosion rate as a function of $HPMC_{tablet}$, the total amount of HPMC remaining in the tablet at a given time.

$$\frac{dHPMC_{tablet}}{dt} = -\frac{V_{MAX} \cdot HPMC_{tablet}}{K_M + HPMC_{tablet}} \quad \text{(Eq. 3)}$$

where V_{MAX} is the maximal HPMC release rate and K_M is the amount of HPMC in the tablet for which the release rate is half of V_{MAX}. The model was implemented using differential equations to facilitate the inclusion of time varying covariate effects such as a change in pH after the gastric emptying to the *in vivo* model.

The presence of an onset on the release of HPMC from the tablet (i.e. initial tablet hydration) was tested using a lag-time.[83] The effect of experimental conditions (mechanical stress, pH and ionic strength) and tablet formulations (proportion of high molecular weight HPMC and calcium hydrogen phosphate (DCP)) were tested on the structural model parameters using the SCM approach. Nonlinear relationships were evaluated using power and Michaelis-Menten type covariate-parameter relationships upon the linear covariate inclusion by the SCM.

In vivo tablet erosion

Clinical data

In a crossover design, five healthy subjects received formulations no. 1 and 2 under fasting status and formulations no. 3 and 4 under both fasting and postprandial status.[82] MMM measurements were used to monitor the tablets location in the GI tract (i.e. stomach, small intestine or colon) and to quantify their erosion. Food and fluid intakes were standardized throughout the duration of the study. MMM measurements were carried out until the net magnetization of a tablet was below 15% of its initial value, but no longer than 14 h post administration.

In vivo model development

The selected *in vitro* model was used as a starting point for the *in vivo* model development. The *in vitro* model parameters were fixed to their final estimates and the GI tract tablet location (MMM data) was used as a time-varying covariate to dynamically adjust the local pH and the mechanical stress in the model.

The erosion rate appeared to vary throughout the small intestine, thus three alternative approaches were tested to split the small intestine location into its proximal and distal parts, either by: 1) using the fractional length of the sections and the individual transit times, 2) estimating a delay after the individual gastric emptying time or 3) setting this delay to one hour as reported by others[8]. The resulting GI location (i.e. stomach, proximal small intestine, distal small intestine or colon) was then used in the model to dynamically adjust the properties of the tablet environment.

Within each GI location, the pH distribution (mean and standard deviation) was set to literature values.[84,85] The extent of the mechanical stress on the tablets was estimated and expressed as USP2 apparatus rotation speed unit equivalent (i.e. rpm). For formulation no. 3 and 4, a postprandial effect was tested by adjusting the distribution of pH values in the stomach; the postprandial effect in other GI segments was assumed to be negligible. A potential postprandial effect was also tested on the mechanical stress in the stomach.

Simulation of the *in vivo* tablet erosion

Model simulations were performed to illustrate the expected *in vivo* HPMC release time profile for different formulations and prandial statuses. New MMM GI location profiles were simulated using a previously published Markov model.[9] The HPMC release profiles were then simulated using the newly generated GI location profiles into the *in vivo* tablet erosion model.

Gastric emptying and bile acids EHC

Clinical data

Acetaminophen (i.e. gastric emptying marker) data were obtained from 33 subjects with type 2 diabetes (T2D) and 33 non-diabetic control. In a crossover study design separated by washout periods, subjects were successively administered: water, three different glucose solutions, and three isocaloric test drinks with low, medium and high fat content (*Table 5*). Gallbladder volumes, plasma CCK and individual bile acids concentrations were also measured in the individuals (15 T2D and 15 controls) who received the 75-g glucose solution and the fat-based test drinks. Acetaminophen, CCK and individual bile acids plasma concentrations were collected repeatedly from 20 min before and up to 4 h after the administration of the test drinks; gallbladder volume was measured from 10 min before and up to 60 min after. TBA concentrations were determined by calculating the molar sum of the 12 most common bile acids.

Table 5. *Properties of the test drinks*

Test drink	Water	OGTT 25 g	OGTT 75 g	OGTT 125 g	Low fat	Medium fat	High fat
Volume (mL)	100	300	300	300	350	350	350
Carbohydrate (g)	0	25	75	125	107	93	32
Protein (g)	0	0	0	0	13	11	3
Fat (g)	0	0	0	0	2.5	10	40
Energy (kcal)[a]	0	100	300	500	503	506	500

OGTT: oral glucose tolerance test. [a] Caloric content calculated using 4 kcal/g for carbohydrates and proteins and 9 kcal/g for fats.[86]

Gastric emptying model

Published population models were used as starting point for the description of acetaminophen's PK.[87–89] The acetaminophen absorption rate constant (K_A) was implemented using a frequentist prior from a published study to allow its distinction from the gastric emptying rate constant (K_G).[47,72] The postprandial effect on the gastric emptying rate was implemented using a feedback from

the caloric content of the upper small intestine; linear and nonlinear (Michaelis-Menten and sigmoidal) functions were evaluated.[90] Delays in the initial phase of gastric emptying were evaluated on all test drink with a lag-time and an onset function.[91] Presence of a saturable first-pass acetaminophen metabolism was evaluated using a Michaelis-Menten type function. Saturable absorption of nutrients from the upper small intestine was implemented using published parameter values for glucose.[87] An SCM approach was used to evaluate the reported effects of gender, obesity, and T2D on the rate of gastric emptying.[34–37]

Sensibility of the model to fixed parameter values (i.e. K_A, nonlinear glucose absorption parameters) was evaluated though a sensitivity analysis where the value of the fixed parameters was sequentially modulated by ±25%, and the predictions of the new model compared to the reference.

CCK model

Graphically, the postprandial plasma CCK concentrations displayed two distinct peaks: a first high and narrow (CCK_F) and a second lower and wider (CCK_L).[92,93] Two indirect response models were used to describe the changes in CCK_F and CCK_L plasma concentrations. The postprandial effect was implemented via stimulation of the rates of CCK_F and CCK_L production. Alternatively, precursor pools were tested on each indirect response model to mimic exhaustion of the secretion process. In this case the postprandial effect was implemented as an increase in the rate constant of release from the pool into the plasma.[94] The effect on CCK secretion was tested through linear and nonlinear (Michaelis-Menten and sigmoidal) functions of the amount of nutrients in duodenum for CCK_F and upper jejunum for CCK_L.[14] The relative potency of proteins and carbohydrates to trigger the release of CCK were evaluated in regards to fats.[95] Nutrients in duodenum and upper jejunum were nonlinearly absorbed as described for the gastric emptying model.[87] The total plasma CCK concentrations were obtained by summing the predicted CCK_F and CCK_L concentrations. An SCM approach was used to explore the possible effects of age, gender, body weight, body mass index, and T2D on key structural parameters.

Bile EHC model

TBA distribution model

Published data on radiolabeled total cholic acid serum concentrations following an intravenous administration were used to develop the TBA distribution model; assuming a similar distribution between TBA and total cholic acid.[50] One- and two-compartment models with elimination mediated through a liver compartment were compared. The Small *et al.*'s equation was used for liver volume calculations.[96]

TBA EHC integrated modeling framework

The modeling framework was designed around the key physiological components of the EHC of TBA. The gallbladder volume dynamics was characterized by an indirect response model. Two alternative emptying mechanisms were tested; gallbladder emptying was either driven by 1) the predicted plasma CCK concentrations, or 2) a signal of the nutrients in the upper small intestine.[97] In both alternatives, the effect on gallbladder emptying was tested through linear and nonlinear (Michaelis-Menten and sigmoidal) functions of the emptying signal.

Postprandial TBA plasma concentrations were characterized by two distinct peaks, which were assumed to be associated with the recirculation of bile acids.[22] A transient postprandial gallbladder refilling period was tested to allow the model to predict these double peaks despite a sustained emptying signal.[98] The size of the TBA pool was assumed to be constant (i.e. no loss to the colon nor *de novo* production by the liver). The liver compartment was implemented as a well-stirred type model, for which the volume was computed using Small *et al's.* equation.[96,99] The E_H determined the TBA fraction arriving to the liver and returning to the gallbladder. Constant and concentration-dependent Michaelis-Menten E_H functions were evaluated. The TBA fraction escaping E_H was directed to the plasma compartment.

Sensitivity of the model to fixed parameter values was evaluated through simulations and re-estimation similarly to the method described for the gastric emptying model.

Treatment of Indian children with TB

Clinical data

Data were obtained from 161 treatment-naive Indian children (1–15 years old), 84 had drug-sensitive TB monoinfection and 77 had TB-HIV coinfection.[56,57] All children received a thrice-weekly course of anti-TB treatment for 6 months as per the previous RNTCP guidelines.[63] Eligible children were also given antiretroviral treatment. The PK study was conducted at least two weeks after initiation of the treatment. INH, RIF and PZA concentrations were collected at 0, 2, 4, 6 and 8h post dose. After 6 months, the treatment outcome was reported as unfavorable (i.e. treatment failure or death), favorable (i.e. treatment completion or cure) or unknown (i.e. lost during follow-up).[56,57]

PK models

To describe the PK of INH, RIF and PZA, one- and two-compartment models with linear/saturable elimination and constant/saturable relative bioavailability were compared. K_A estimations were supported by the use of frequentist

priors, which were based on literature values.[71,72,100] Delays in drug absorption were tested using chains of transit compartments.[71,101] Age-related maturation parameters for INH and RIF clearances and RIF absorption delay were fixed to literature values.[71] For subjects with the rapid INH acetylator polymorphism (i.e. high metabolism), the effect was tested on the clearance and the relative bioavailability.[71,102] An SCM approach was used to investigate the effects of covariates on the drug's apparent clearances, distribution volumes and relative bioavailabilities.

Treatment outcome model

The probability of unfavorable treatment outcome ($P_{unfavorable}$) was modeled with a logistic regression model; subjects with unknown treatment outcome (n = 19) were excluded from this analysis. An SCM was used to evaluate the effect of INH, RIF, PZA drug exposures (implemented as the total weekly area under the concentration-time curve (AUC)) and subject characteristics (e.g. HIV status, demographics, etc.) as predictors of $P_{unfavorable}$.

RNTCP dosing regimens

The PK-PD model was used to predict $P_{unfavorable}$ under the previous (thrice-weekly) and the new (daily) RNTCP dosing regimens. Drug exposures were simulated 1,000 times for children within the respective RNTCP pediatric weight ranges. $P_{unfavorable}$ was computed for each simulated individual before being summarized by weight bands and by each predictor of the treatment outcome. Optimized doses were proposed for each of the new RNTCP weight bands based on a $P_{unfavorable}$ of 5% or less.[65,103]

Results

In vitro–in vivo modeling of ER formulations

In vitro tablet erosion

The Michaelis-Menten model appropriately described the HPMC release rate of the four formulations under all studied experimental conditions (*Figure 5*). Parameter estimates are reported in *Table 6*.

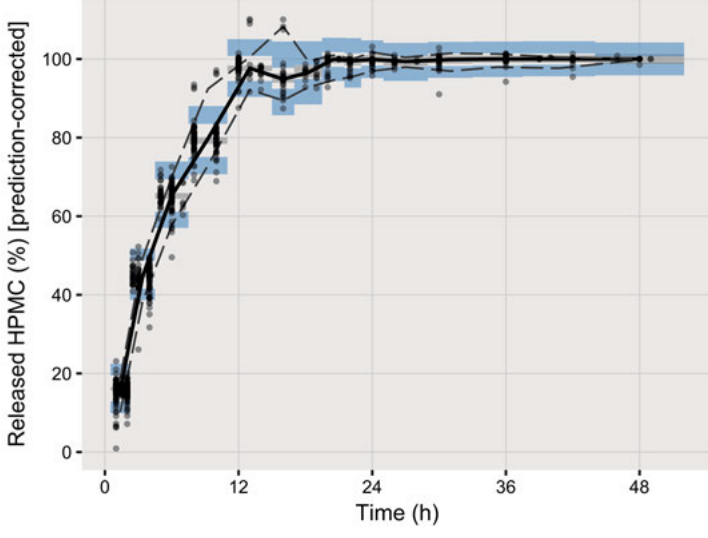

Figure 5. Prediction-corrected VPC of the *in vitro* released HPMC time course for all formulations and experimental conditions. The median *(bold line)*, 5th and 95th percentiles *(dashed lines)* of the observed data are compared to the 95% confidence intervals for the median *(grey areas)*, the 5th and 95th percentiles of the simulated (n = 1,000) data *(blue areas)*.

Table 6. *Parameter estimates of the in vitro model*

Parameter (units)	Estimate (RSE%)[c]
V_{MAX} (mg_{HPMC}/h)	22.0 (2.5)
K_M (mg_{HPMC})	34.2 (6.1)
Lag-time (h)	0.179 (15)
$MK4M_{50\text{-}VMAX}$ (% w/w)	18.7 (3.5)
$S_{DCP\text{-}KM}$ (% w/w^{-1})[a]	0.0522 (33)
$S_{DCP\text{-}VMAX}$ (% w/w^{-1})[a]	0.0332 (24)
$S_{pH\text{-}KM}$ (pH $unit^{-1}$)[a]	0.0935 (15)
$S_{pH\text{-}VMAX}$ (pH $unit^{-1}$)[a]	–0.0319 (24)
$S_{rpm\text{-}VMAX}$ (rpm^{-1})[a]	0.0115 (2.9)
BTV V_{MAX} (CV %)	5.96 (17)
Additive error (mg_{HPMC})[b]	1.95 (14)

[a] effect of covariates reported as relative the change in the model parameter typical value for each unit change of the covariate in reference to its median; [b] reported on the standard deviation scale; [c] reported on the approximate standard deviation scale.

The introduction of a lag-time (11 min) describing the initial tablet hydration significantly improved the fit of the model. Effects of pH, mechanical stress, the proportions of high molecular weight HPMC and DCP in the tablet were found on V_{MAX} (*Equation 4*), while K_M was impacted by pH and the proportion of DCP in the tablet (*Equation 5*). No significant effect of the ionic strength was detected.

$$V_{MAX_i} = TV_{VMAX} \cdot E_{rpm\text{-}VMAX} \cdot E_{pH\text{-}VMAX} \cdot E_{DCP\text{-}VMAX} \cdot E_{MK4M\text{-}VMAX} \cdot e^{\eta_{i-VMAX}} \quad \text{(Eq. 4)}$$

$$K_M = TV_{KM} \cdot E_{pH\text{-}KM} \cdot E_{DCP\text{-}KM} \quad \text{(Eq. 5)}$$

where TV_{VMAX} and TV_{KM} are the typical (i.e. formulation no. 3, pH 6.8 and mechanical stress of 50 rpm) parameter values of V_{MAX} and K_M. η_i represents the BTV on V_{MAX}. $E_{rpm\text{-}VMAX}$, $E_{pH\text{-}VMAX}$, $E_{DCP\text{-}VMAX}$ and $E_{MK4M\text{-}VMAX}$ are respectively the relative effects of mechanical stress, pH, DCP and high molecular weight HPMC on TV_{VMAX}. $E_{pH\text{-}KM}$ and $E_{DCP\text{-}KM}$ are respectively the relative effects of pH and DCP on K_M. $E_{MK4M\text{-}VMAX}$ was best described by a saturable relationship (*Equation 6*) which resulted in a significant improvement of the fit over a linear relationship:

$$E_{MK4M\text{-}VMAX} = 1 - \frac{MK4M}{MK4M_{50\text{-}VMAX} + MK4M} \quad \text{(Eq. 6)}$$

where MK4M is the proportion of high molecular weight HPMC and $MK4M_{50\text{-}VMAX}$ the MK4M leading to a decrease by half of $E_{MK4M\text{-}VMAX}$. BTV was only supported on V_{MAX} and was minor (5.96% coefficient of variation (CV)). The RUV was best described by an additive error model. A visual representation of the effect of the included covariates on the released HPMC is provided in *Figure 6.*

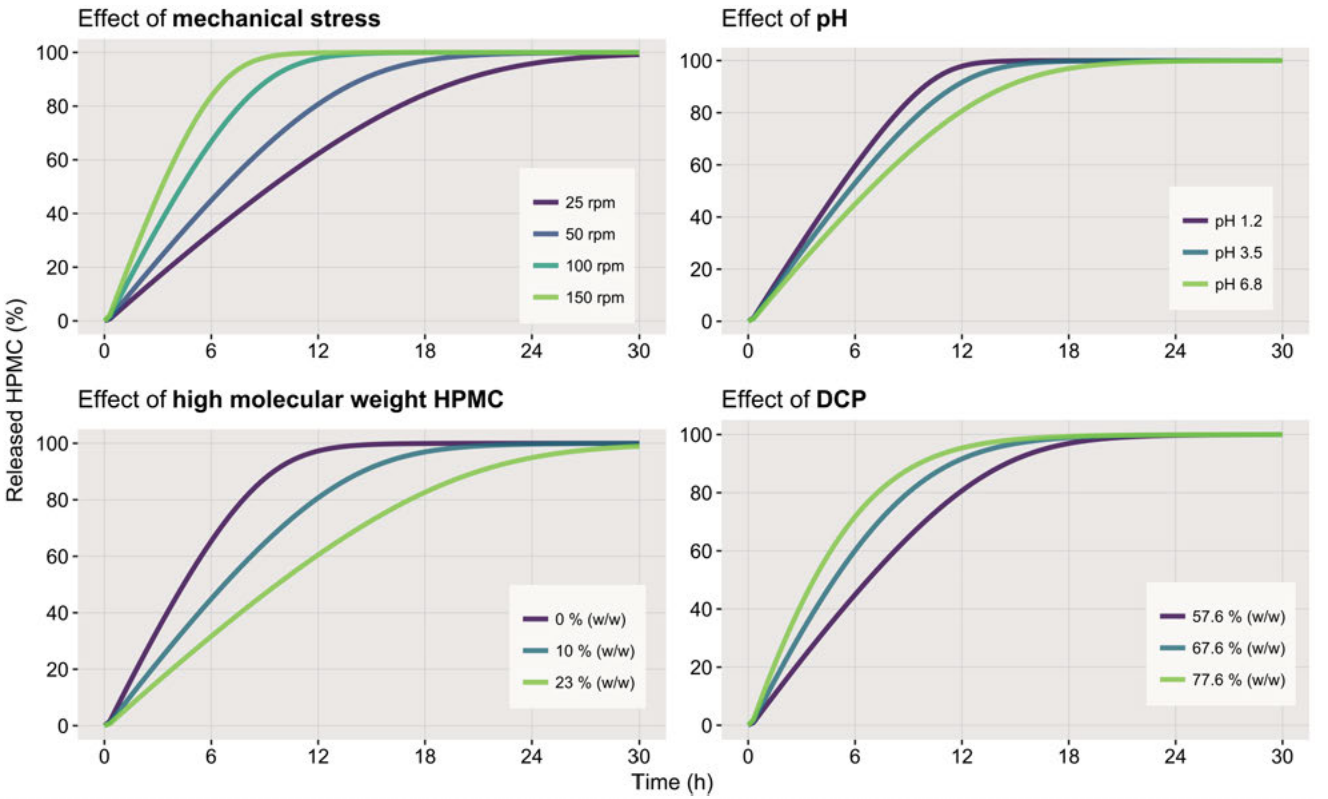

Figure 6. Illustration of the predicted *in vitro* effect of: mechanical stress *(top left)*, pH *(top right)*, high molecular weight HPMC *(bottom left)* and DCP *(bottom right)* on the released HPMC time profiles.

In vivo tablet erosion

Overall, the *in vivo* tablet erosion model had good predictive performances (*Figure 7*). However, the model systematically overpredicted the formulation no. 4 (i.e. with lowest HPMC content) under the fasting status. The data for formulation no. 4 under fasting status were thus excluded during the final parameters estimation, but were used for diagnostics and simulations. This approach prevented the introduction of an estimation bias on the model parameters.

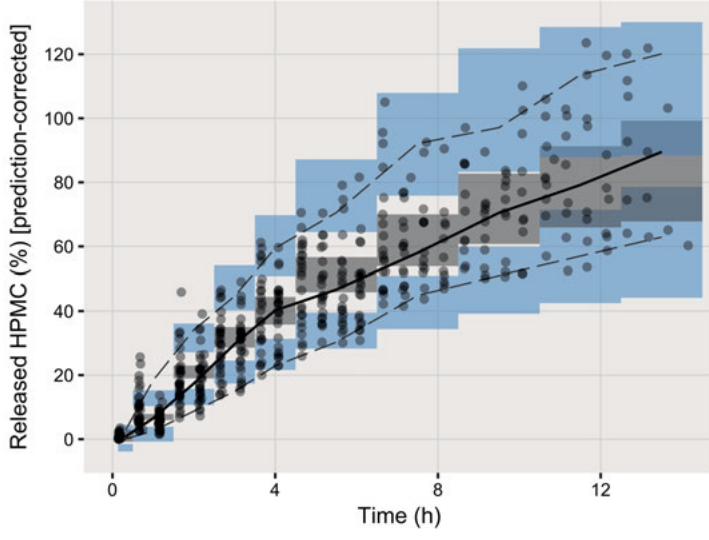

Figure 7. Prediction-corrected VPC of the *in vivo* released HPMC time profiles for all formulations and prandial statuses combined. The median *(bold line)*, 5th and 95th percentiles *(dashed lines)* of the observed data are compared to the 95% confidence intervals for the median *(grey area)*, the 5th and 95th percentiles of the simulated (n = 1,000) data *(blue areas)*.

The model fit was significantly improved by the small intestine segmentation into its proximal and distal parts. The best fit was achieved when the transfer between proximal and distal parts was set to one hour after the gastric emptying. The mechanical stress parameters were thus estimated for stomach (39.5 rpm), proximal small intestine (93.3 rpm), distal small intestine (31.1 rpm) and colon (9.99 rpm). The re-estimation of the lag-time (25 min) further improved the model fit. BSV and BOV were estimated on V_{MAX} to 14.9% CV and 15.5% CV respectively, but neither were supported on K_M. In the post-prandial state the stomach pH was increased, however a change in the mechanical stress was not supported by the data. The RUV was best described by a combined error model. Model simulations illustrating the predictions of the selected *in vivo* tablet erosion model under different formulations and prandial statuses are presented in *Figure 8.*

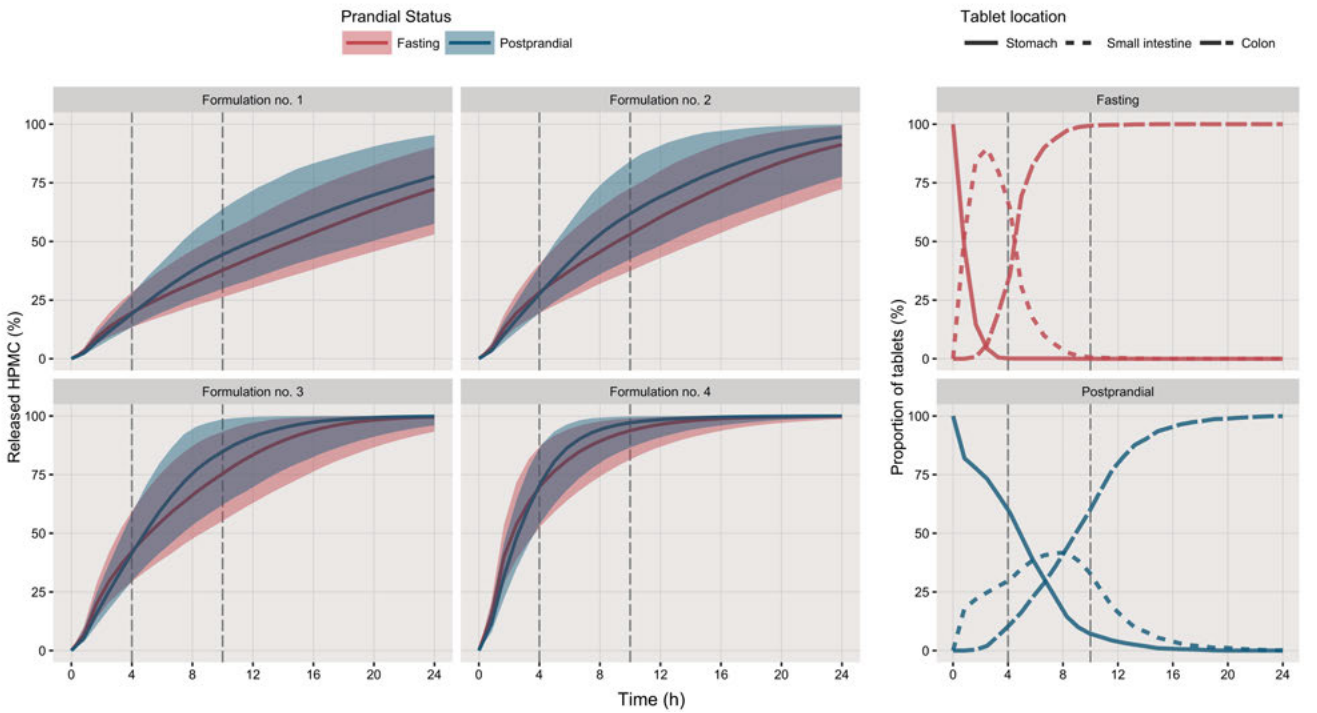

Figure 8. Left: Simulated *in vivo* released HPMC time profiles as a function of prandial status *(color)* and formulation *(panel)*. Vertical dashed lines represent the time of subsequent meal intake (i.e. lunch +4 h and dinner +10 h) for both the fasting and postprandial conditions. *Right:* Graphical representation of the proportion of simulated tablet location in each GI segment *(line type)* as function of the prandial status *(color)*. These tablet locations were used in the *in vivo* model to generate the released HPMC profiles.

Gastric emptying and bile acids EHC

A schematic representation of the selected TBA EHC modeling framework is provided in *Figure 9*, parameter estimates are provided in *Table 7* and VPC in *Figure 10.*

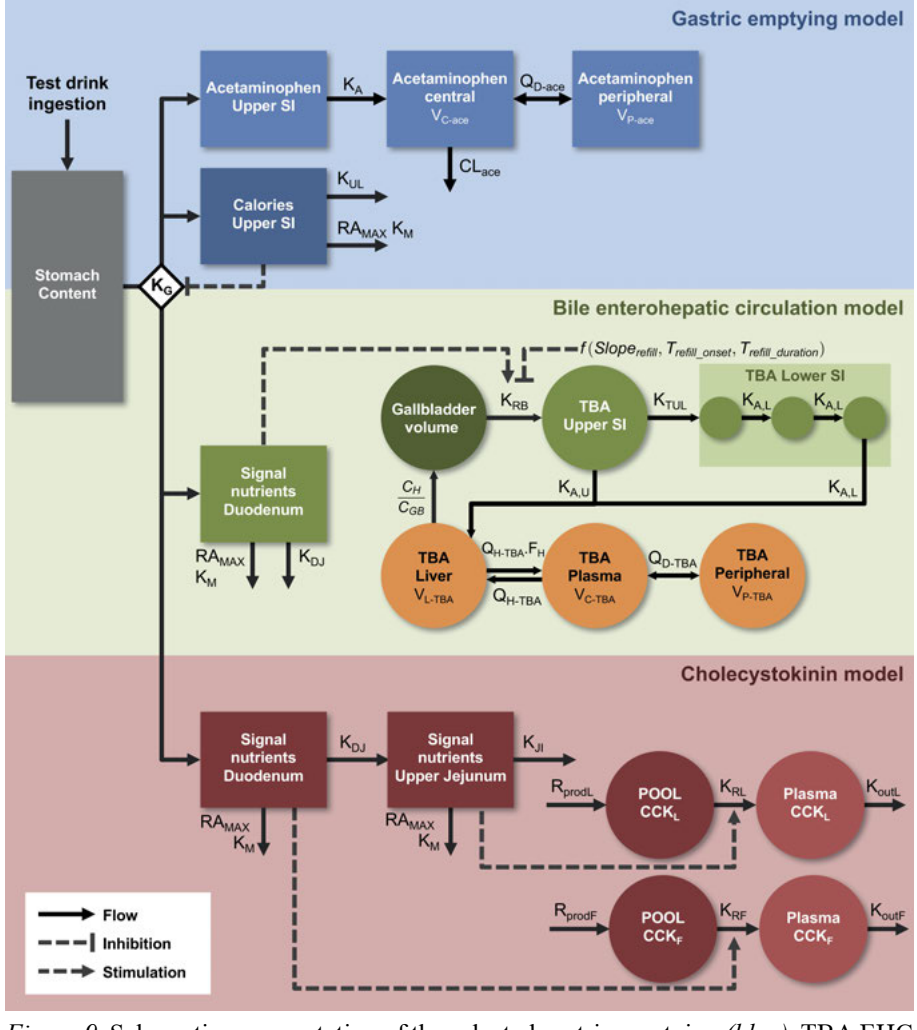

Figure 9. Schematic representation of the selected gastric emptying *(blue)*, TBA EHC *(green)* and CCK *(red)* models.

Table 7. *Parameter estimates for the selected TBA EHC modeling framework*

Gastric emptying model			**Gallbladder emptying model**			**TBA EHC model**		
Parameters (unit)	Estimates (RSE)	Var[a] CV% (RSE)	Parameters (unit)	Estimates (RSE)	Var[a] CV% (RSE)	Parameters (unit)	Estimates (RSE)	Var[a] CV% (RSE)
CL_{ace}/F (L/min)[b]	0.441 (2.5)		Base GB (mL)[b]	29.4 (3.5)	27 (7.5)	HL_{TUL} (min)	56.2 (35)	
$V_{C\text{-}ace}/F$ (L)[b]	19.5 (12)	68 (32)	HL_{RB} (min)	918 (9.4)	92 (8.3)	F_{AU} (%)	20.6 (24)	0.65 (15)[d]
$V_{P\text{-}ace}/F$ (L)[b]	48.1 (4.4)		$Slope_{efat}$	86.7 (13)	100 (14)	OGTT–F_{AU} (%)	+132 (14)	
$Q_{D\text{-}ace}/F$ (L/min)[b]	1.56 (5.6)		Age–$Slope_{efat}$ (%/y)	-2.69 (80)		$MTT_{A,L}$ (min)	111 (14)	49 (16)
F_1	1 fixed	22 (12)	RA_{MAX} (kcal/min)	2.29 fixed		Carbs–$MTT_{A,L}$ (%/g)	+0.637 (27)	
HL-K_A (min)[c]	8.19 (8.6)		K_{50} (kcal)	25.1 fixed		Female–$MTT_{A,L}$ (%)	-29.1 (37)	
K_{G0} (min^{-1})	1.06 (21)	155 (17)	HL_{DJ} (min)	2.42 (17)		E_H (%)	64.0 (4.5)	0.58 (17)[d]
K_{UL} (min^{-1})	0.0266 (10)	56 (21)	P_{carb} (%)	5.67 (20)		High fat–E_H (%)	-31.2 (35)	
SLP_{CAL}	-0.0173 (8.8)	19 (31)	P_{prot} (%)	86.9 (25)		$Q_{H\text{-}TBA}$ (L/min)[b]	1.5/2 fixed (fasting/fed)	
Female–SLP_{CAL} (%)	+40.7 (18)		$Slope_{refill}$	0.149 (17)		$V_{C\text{-}TBA}$ (L)[b]	2.84 fixed	
SIG	0.285 (17)		T_{refill_onset} (min)	25.3 (13)	72 (14)	$V_{P\text{-}TBA}$ (L)[b]	4.07 fixed	
T_{50OGTT} (min)	15.7 (13)		$T_{refill\_duration}$ (min)	151 (12)	31 (30)	$Q_{D\text{-}TBA}$ (L/min)[b]	0.173 fixed	
T_{50Fat} (min)	23.1 (13)					TBA conc. GB (mM)	113 fixed	
			Add. Err. (mL)	2.01 (9.8)				
Prop. Err. (%)	14.8 (2.3)		Prop. Err. (%)	10.4 (7.6)		Prop. Err. (%)	31.5 (3.4)	

[a] The variability herein represents the total variability i.e. the sum of the BSV and BOV reported on the approximate standard deviations scale; [b] Parameter allometrically scaled in reference to a 70-kg individual and using an allometric exponent of 1 for volumes and ¾ for clearances; [c] Parameter with prior information ($HL\text{-}K_{A\_prior}$ = 6.8 ± 0.9 min); [d] Standard deviation for additive variability on the logit scale.

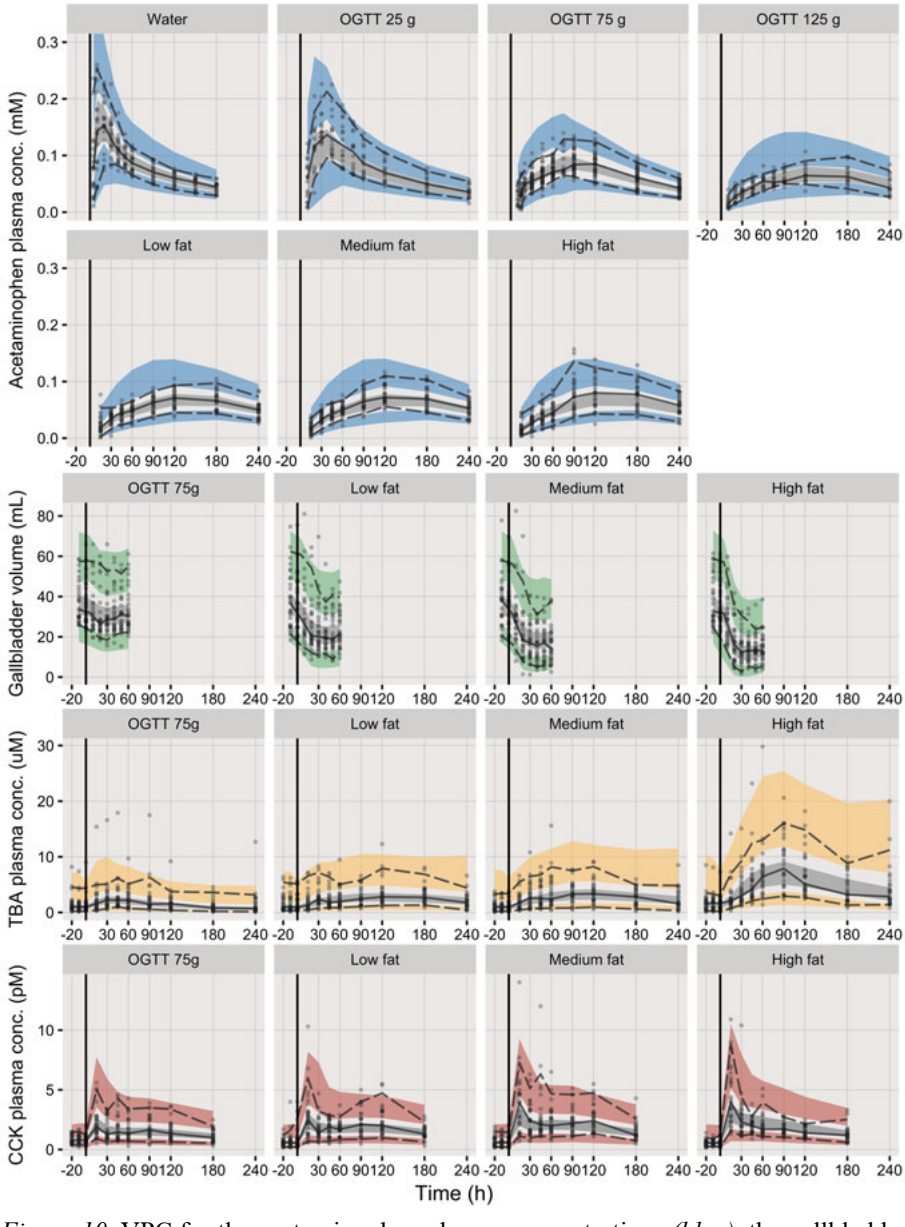

Figure 10. VPC for the acetaminophen plasma concentrations *(blue)*, the gallbladder volumes *(green),* the TBA plasma concentrations *(orange)* and the CCK plasma concentrations *(red)* stratified by test drinks. For each panel, the median *(bold line)*, 5th and 95th percentiles *(dashed lines)* of the observed data are compared to the 95% confidence intervals for the median *(grey area)*, the 5th and 95th percentiles of the simulated (n = 1,000) data *(colored areas)*. The vertical lines mark the intake of the test drinks. OGTT: oral glucose tolerance test.

Gastric emptying model

In total 183 individual profiles and 1,615 acetaminophen concentrations were used in the development of the gastric emptying model. One subject was excluded due to the absence of acetaminophen dose on all studied occasions.

The gastric emptying rate was regulated by the caloric content in the upper small intestine (CAL_{USI}) as shown in *Equation 7*.

$$K_G = K_{G0} \cdot (1 - SLP_{CAL} \cdot CAL_{USI}) \quad \text{(Eq. 7)}$$

where K_{G0} is the basal (i.e. water) gastric emptying rate constant, SLP_{CAL} the slope of the linear feedback. The onset function (*Equation 8*) gave better performance and stability (i.e. no change point) than the lag-time; improvements were also noted in the initial phase of gallbladder emptying.

$$GE_{onset}(t) = \frac{1}{1 + e^{-SIG \cdot (t - T_{50})}} \quad \text{(Eq. 8)}$$

where SIG is the sigmoidicity factor, t the time after the last dose and T_{50} the time to 50% of the maximal onset. Estimation of different T_{50} parameters for fat–based (23 min) and non-fat-based (16 min) test drinks significantly improved the model fit. Implementation of a saturable first-pass was not supported by the data; the model fit was however significantly improved by estimating the variability on the relative acetaminophen bioavailability.

The feedback of the caloric content in the upper small intestine on was found to be 40% stronger in women than in men (*Equation 9*):

$$SLP_{CAL_i} = TVSLP_{CAL} \cdot (1 + 0.4 \cdot FEM_i) \cdot e^{\eta_{i-SLP}} \quad \text{(Eq. 9)}$$

where $TVSLP_{CAL}$ is the typical value of SLP_{CAL}, FEM is a variable set to 1 for females and to 0 for males and $\eta_{i\text{-}SLP}$ represents the total variability for SLP_{CAL}. Finally, RUV was best described by a proportional error model.

The sensitivity analysis revealed that the model was not sensitive to changes of ±25% in K_A and the saturable nutrients absorption parameters. Model simulations illustrating the model predictions for different meals are presented in *Figure 11*.

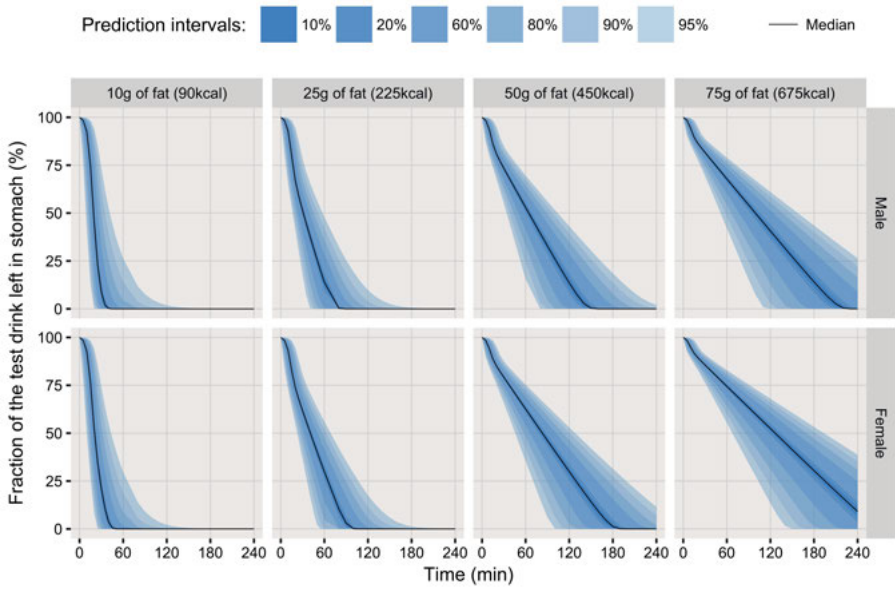

Figure 11. Model-based simulations of the time course of the fraction of a test drink left in stomach, stratified by the caloric content of the test drink and by gender. For each panel, the median *(solid line)* and different prediction intervals *(shaded areas)* were calculated based on 1,000 simulations of the model development dataset.

CCK model

In total 115 individual profiles and 1,150 CCK plasma concentrations were used for the model development. The use of precursor pools for both CCK_F and CCK_L significantly improved the model predictions over simple indirect response models. The estimated pool size was markedly higher for CCK_F (17.1 pM) compared to CCK_L (1.95 pM), but the elimination half-life was markedly shorter (1.95 min vs. 127 min). The CCK_F release was best fitted by a nonlinear function of the signal of nutrients in duodenum, the CCK_L release was on the other hand best fitted by a linear model of the amount of nutrients in the upper jejunum (*Figure 9, Figure 10*). In relation to fat, the potency per gram of carbohydrates to trigger the CCK release was only 10%; estimation of a potency term for proteins was not supported by the data. Furthermore, the relative carbohydrate potency was reduced by -81% in patients with T2D subjects compared to non-diabetic individuals. Due to the complexity of the model, several parameters were poorly estimated and had a high RSE namely: the baseline of CCK_L (125%), the relative potency of carbohydrates (65%), the signal-effect related parameters for the secretion of CCK_F (82%) and CCK_L (54%). The mean residence time of nutrients in the duodenum and in the upper jejunum were also poorly estimated and hence fixed to published values (12 min and 90 min respectively).[87] Finally, the RUV was best described by a proportional error model.

Bile EHC model

In total 115 individual profiles, 920 gallbladder volumes and 1,236 TBA plasma concentrations were used for the model development. One outlier sample (~27 times higher than baseline) was excluded from the analysis.

The TBA distribution was best described by a two-compartment model. The model predictions were in good agreement with the total cholic acid data from the radiolabeled study.[50] The typical volume of central and peripheral compartments, and the inter-compartmental clearance values indicated a rapid but contained distribution (*Table 7*).

The model poorly predicted the data when the predicted CCK concentrations were as single driver of the postprandial gallbladder emptying. Nevertheless, when the gallbladder emptying was mediated by a fat equivalent signal from the nutrients in duodenum ($efat_{duod}$; *Equation 10*), the model properly fitted the data (*Figure 9*, *Figure 10*).

$$\mathrm{efat_{duod}}(t) = \left(\mathrm{g_{carb,duod}}_t \cdot \mathrm{P_{carb}}\right) + \left(\mathrm{g_{prot,duod}}_t \cdot \mathrm{P_{prot}}\right) + \mathrm{g_{fat,duod}}_t \quad \text{(Eq. 10)}$$

where t is the time since the intake of the test drink, $g_{carb,duod}$, $g_{fat,duod}$, $g_{prot,duod}$ are the grams of carbohydrates, fats and proteins in the duodenum, P_{carb} and P_{prot} represent the potency of carbohydrates and proteins in relation to fat (i.e. $P_{fat} = 1$). A linear function best described the relationship between the rate of gallbladder emptying ($R_{GB,out}$) and $efat_{duod}$ (*Equation 11*). Furthermore, the addition of a postprandial gallbladder refilling function (GB_{refill}; *Equation 12*) significantly improved the model fit by refining the predictions of the double peaks seen in the TBA plasma concentration time-course.

$$\mathrm{R_{GB,out}}(t) = \mathrm{GB_{vol}}_t \cdot \mathrm{K_{RB}} \cdot (1 + \mathrm{Slope_{efat}} \cdot \mathrm{efat_{duod}}_t) \cdot \mathrm{GB_{refill}}_t \quad \text{(Eq. 11)}$$

where GB_{vol} is the gallbladder volume, $Slope_{efat}$ is the slope of the effect of $efat_{duod}$ and GB_{refill} defined as:

$$\mathrm{GB_{refill}}(t) = 1 - \frac{1}{1 + \mathrm{e}^{-\mathrm{Slope_{refill}} \cdot (t - \mathrm{T_{refill\_onset}})}} + \frac{1}{1 + \mathrm{e}^{-\mathrm{Slope_{refill}} \cdot (t - \mathrm{T_{refill\_onset}} - \mathrm{T_{refill\_duration}})}} \quad \text{(Eq. 12)}$$

where $Slope_{refill}$ is the steepness of the onset and offset of gallbladder refilling, T_{refill_onset} is the time to 50% of maximal gallbladder refilling onset and $T_{refill\_duration}$ the duration for which gallbladder refilling at more than half of its maximal effect. Estimates for these parameters indicated an early (25 min) and sustained (151 min) refilling period with progressive onset and offset phases. Despite an effect of age on $Slope_{efat}$ (-2.69%/yr), the variability on the gallbladder emptying parameters was substantial (*Table 7*).

The TBA fraction absorbed in the upper small intestine (F_{AU}) was found to be 20.6% for fat-containing drinks and 47.8% for the 75-g oral glucose toler-

ance test (OGTT). Splitting the lower small intestine into three sub-compartments and restraining the absorption to the terminal end significantly improved the model fit. The mean transit time of TBA throughout the lower small intestine (111 min) was shorter in females (-29.1%) and positively correlated with the amount of ingested carbohydrates (+0.637%/g). E_H was found to be constant (64.0%), but reduced with the high fat test drink (44.0%). T2D was not associated with any significant change in any of the model parameters.

Estimating the covariance between the individual model parameters greatly improved the model fit. The RUV of the gallbladder data was best described by a combined error model, while a proportional error model best suited the TBA plasma concentration data.

The sensitivity analysis revealed that the model was not sensitive to changes of ±25% in the distribution clearance, central and peripheral volumes of TBA distribution. For the TBA concentration in gallbladder or the hepatic clearance, small differences could be seen graphically in the median of the predictions when comparing to the reference model. Although, the predictions medians of the test models were similar to the reference model after a re-estimation step. Model simulations illustrating the model predictions for different meals are presented in *Figure 12*.

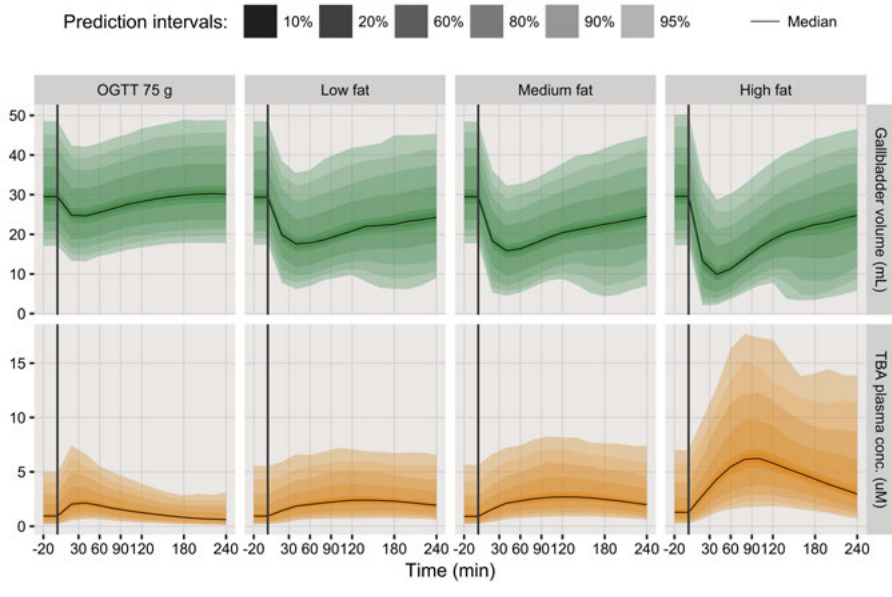

Figure 12. Model-based simulations of the gallbladder volume *(green)* and TBA plasma concentration *(orange)* time-courses stratified by the test drink. For each panel, the median *(solid line)* and different prediction intervals *(shaded areas)* were calculated based on 1,000 simulations of a typical male individual of 70 kg, 1.7 m height and 64 years old. The vertical lines mark the intake of the test drinks. OGTT: oral glucose tolerance test.

Treatment of Indian children with TB

PK models

In total, 805 plasma concentrations were collected for INH, 794 for RIF, and 720 for PZA. Samples below the detection limit (INH: 125, RIF: 105, PZA: 67; mainly represented by through concentrations) were excluded from the analysis.

The INH disposition was best described by a two-compartment model whereas a one-compartment best suited RIF and PZA. Regardless, all three drugs had PK models as highlighted hereafter. Delays in the drugs' absorption were best predicted by chains of transit compartments. BSV in the mean transit time (INH 49.8%, RIF 64.4%, PZA 42.5% CV), apparent clearances (INH 74.2%, RIF 45.4%, PZA 37.4% CV) and volumes (INH 44.9%, RIF 37.3%, PZA 34.4% CV) parameters were substantial. Furthermore, clearances and volumes were highly correlated (INH 86.9%, RIF 78.8%, PZA 51.7%).

Through the covariate search, a strong relationship was found between the relative bioavailability of all three drugs and the individuals' total body weight. This relationship was described by a power-type function where the exponent was estimated, indicating that small children have the lowest relative bioavailability. Effects of HIV were found on RIF clearance (+31.6%), RIF relative bioavailability (-41.5%), and INH relative bioavailability (-19.5%), leading to an additional decrease to the RIF and INH exposures. Furthermore, HIV coinfection was associated with a substantial increase in the BSV on the RIF clearance (+74.0%) and volume of distribution (+106%) parameters. RUV was best described by a combined error model for INH and additive error models for RIF and PZA.

The capacity of the developed INH, RIF and PZA models to predict the drug exposures was evaluated via posterior predictive checks (*Figure 13*).

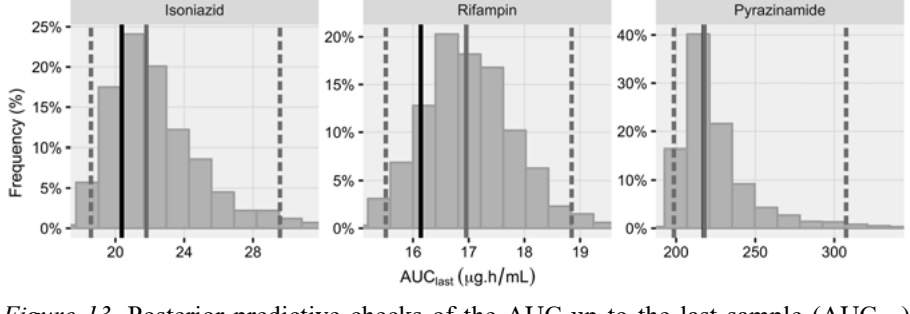

Figure 13. Posterior predictive checks of the AUC up to the last sample (AUC_{last}) population medians obtained from simulations (n = 1,000) of the isoniazid *(left panel)*, rifampin *(middle panel)*, and pyrazinamide *(right panel)* models. Model predictive performances are evaluated by comparing the AUC_{last} population median, calculated from the observed concentrations *(solid black lines)*, to the median *(solid grey lines)* and 95% confidence interval *(dotted grey lines)* of the AUC_{last} population medians calculated for each simulated dataset.

Treatment outcome model

In total, the treatment outcome was favorable in 109 (68%), unfavorable in 33 (20%) and unknown in 19 (12%) children. Subjects with unknown treatment outcome were not associated with any specific characteristics and were excluded from the analysis.

The AUC was retained over the peak concentration as a marker of drug exposure, both metrics were however highly correlated (R^2 for INH: 78%, RIF: 91% and PZA: 77%). Through the covariate search, RIF exposure (9.81–231 µg.h/mL range) was found to be the only independent predictor of $P_{unfavorable}$. No statistically significant effects of the subject characteristics, INH or PZA exposures (INH: 3.89–346 µg.h/mL and PZA: 351–2780 µg.h/mL) could be detected on $P_{unfavorable}$. The model-predicted odds ratio was 2.27 (95% confidence interval: 1.27–4.05) for TB-HIV coinfection in reference to TB monoinfection (median AUC: 36.8 µg.h/mL vs. 93.6 µg.h/mL) and 1.68 (95% confidence interval: 1.16–2.41) for children in the 6–10 kg weight band in reference to children in the 26–30 kg weight band (median AUC: 60.7 µg.h/mL vs. 96.5 µg.h/mL) due to decreased RIF exposures.

The model predicted that the weekly RIF exposure should be at least 185 µg.h/mL in order to achieve a median target $P_{unfavorable}$ of 5% or less. The relationship between the RIF exposure and the $P_{unfavorable}$ is illustrated in *Figure 14*.

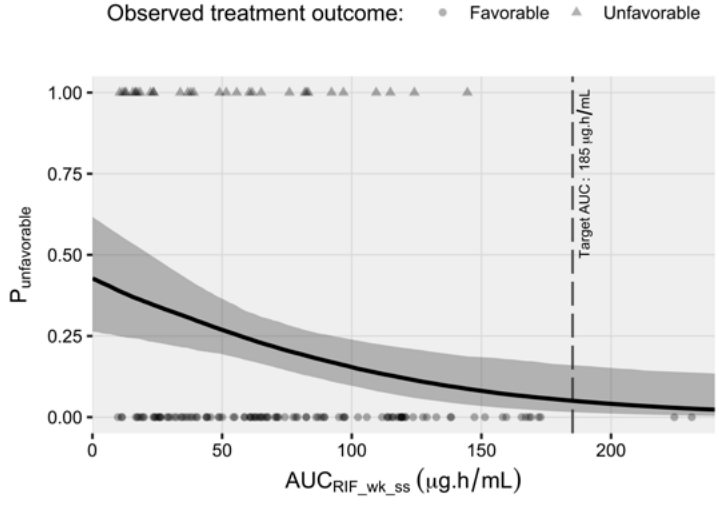

Figure 14. Median (*line*) and 95% confidence interval (*shaded area*) of the model simulated $P_{unfavorable}$ vs. the weekly RIF exposure at steady state ($AUC_{RIF\_wk\_ss}$). The vertical line marks the defined target $AUC_{RIF\_wk\_ss}$ associated with $P_{unfavorable}$ of 5%.

RNTCP dosing regimens

Model-based simulations of the previous and new RNTCP dosing regimens were performed. An increased $P_{unfavorable}$ was revealed for children with low body weight (6–10 kg for previous and 4–7 kg for new RNTCP guidelines) or TB-HIV coinfection due to suboptimal RIF doses in these sub-groups (*Figure 15*). Among the children with TB-HIV, the median $P_{unfavorable}$ was as high as 35%. Although, reasonable (i.e. ≤ 5%) $P_{unfavorable}$ is expected for most children with TB monoinfection under the new once-daily RNTCP dosing regimen.

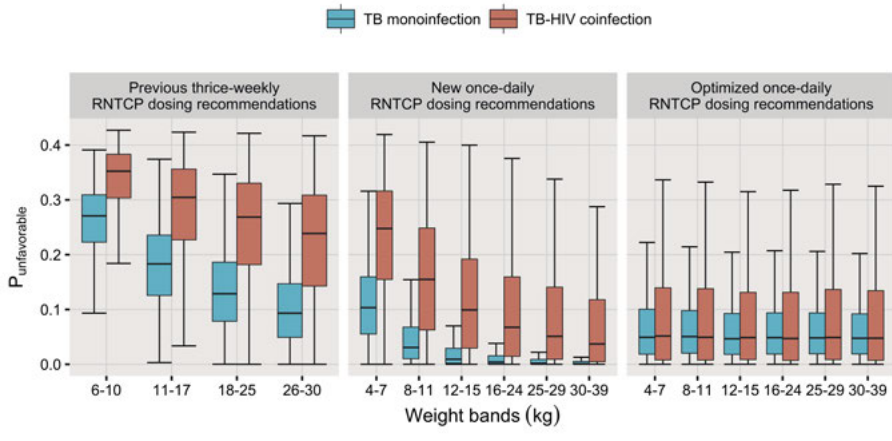

Figure 15. Predicted $P_{unfavorable}$ under previous *(left panel)*, new *(central panel)* and optimized *(right panel)* RNTCP dosing recommendations. RIF weekly exposures at steady state were simulated (n = 1,000) for children within the pediatric RNTCP weight range (i.e. 6–30 kg for previous and 4–39 kg for new and optimized dosing recommendations); $P_{unfavorable}$ distributions were computed for each weight band, and TB-HIV coinfection status.

Optimized daily RIF pediatric doses were computed using the pre-defined weekly target AUC and given different weight bands and HIV coinfection status (*Table 8)*. In comparison to the previous and new RNTCP guidelines, the predicted optimized doses were mostly increased for children with low body weight (4–7 kg) and especially for children with TB-HIV coinfection, with doses up to 43.4 mg/kg. However, for bigger children (>25 kg), the model predicted that the target could be achieved, even with daily doses as low as 5.2 mg/kg.

Table 8. *Optimized once-daily pediatric dosing regimen for RIF*[a]

Weight band	**TB monoinfection**		**TB-HIV coinfection**	
kg	Dose[b]	$P_{unfavorable}$[c]	Dose[b]	$P_{unfavorable}$[c]
	mg (mg/kg)	median (CI_{95})	mg (mg/kg)	median (CI_{95})
4–7	109 (19.9)	0.0535 (0.0107–0.129)	239 (43.4)	0.0606 (<0.01–0.202)
8–11	126 (13.3)	0.0554 (0.0129–0.126)	275 (28.9)	0.0591 (<0.01–0.196)
12–15	139 (10.3)	0.0506 (0.0107–0.124)	311 (23.0)	0.057 (<0.01–0.18)
16–24	154 (7.7)	0.048 (0.0162–0.101)	346 (17.3)	0.0464 (<0.01–0.149)
25–29	166 (6.2)	0.0484 (0.0106–0.124)	383 (14.2)	0.0492 (<0.01–0.188)
30–39	180 (5.2)	0.0478 (0.0173–0.0966)	404 (11.7)	0.0509 (<0.01-0.142)

[a] Doses given for single drug formulations; [b] Doses in mg/kg calculated using the average total body weight within each weight band; [c] Reported as the median and the 95% confidence interval (CI_{95}) around the simulated medians (n = 1,000).

Discussion

In vitro–in vivo modeling of ER formulations

The work in *Paper I* illustrated how an *in silico* approach could be used to predict the *in vivo* erosion of HPMC matrix tablets under different prandial statuses using *in vitro* dissolution experiment data.

The first step in this approach was to characterize the influential factors of the erosion of HPMC matrix tablets. The identified effects of the experimental conditions (pH and mechanical stress) and tablet formulations (proportion of high molecular weight HPMC and DCP in the tablet) were in line with previous findings (*Figure 6*).[37,39,83,104] Unlike the findings from Bergstrand *et al.*, no significant effect of the ionic strength could be detected despite appropriate *in vitro* experiment design (*Table 4*).[8] These discrepancies could be explained by differences in the HPMC quality and the solubility of the tablet components (i.e. API or filling agent) used in the two studies.[105–107] This finding could be an indication that additional influential factors would need to be characterized and integrated to the model.

In the second step, the *in vitro* model was combined with the tablet MMM GI location data to predict the *in vivo* erosion of the HPMC matrix tablets. Despite a good overall fit of the data (*Figure 7*), the model over-predicted the erosion rate of the formulation no. 4 under fasting status. This may have been caused by a weaker HPMC gel layer when the HPMC tablet content was below 30%. This could also be an indication that not all influential factors of the erosion of HPMC matrix tablets have yet been characterized. Through this approach the mechanical stress was estimated for the different GI location (stomach, proximal/distal small intestine, colon) and expressed as USP2 apparatus rpm equivalent. The mechanical stress estimates were lower than previously reported by Bergstrand *et al* for all GI segments.[8] Yet, in their model the mechanical stress estimates were influenced by the selected value of the ionic strength, unlike the model presented herein where the ionic strength had no impact on the predictions.[8] The tablet environment pH distribution was also dynamically set to literature values based on the GI location of the tablet and the prandial status. The postprandial effect was implemented via a change in stomach pH; an effect on the mechanical stress was not supported by the data.[8]

In the third and last step of the proposed approach, the developed *in vitro-in vivo* model was used to illustrate the predictions with the simulations of different formulation and prandial statuses (*Figure 8*). The model also offers

the opportunity to simulate new scenarios (e.g. new formulations) while accounting for the effect of the different covariates and the sources of variability in the erosion rate.[1] To perform these simulations the developed model was used along with a published Markov model describing the GI transit of solid dosage form under different prandial statuses.[9]

If used along with PK data, the proposed model could be extended to help predict the variability in the absorption profile of API released from ER formulations.[108]

Gastric emptying and bile acids EHC

The work from *Paper II* and *Paper III* described how a modeling framework was developed to predict the postprandial changes in the central trend and variability of gastric emptying, CCK plasma concentrations, gallbladder emptying, and TBA plasma concentrations.

The first step in the development of the framework was to establish a gastric emptying model to predict the rate of nutrients' arrival into the upper small intestine. The amount of nutrients in the upper small intestine was later on used to trigger the release of CCK into the plasma and of the bile flow into the duodenum. Published acetaminophen (i.e. gastric emptying marker) models were used as starting point and estimation of K_G was supported by the use of a literature prior on K_A.[47,87–89] As previously reported for liquid and solid meals, the model predictions were improved by the addition of a postprandial onset of gastric emptying.[47,109] Also in line with previous findings, the gastric emptying rate was function of the caloric content in the upper small intestine independently of the nature of the nutrients.[90,110] Osmolality has also been suggested to play a role in the regulation of gastric emptying[11], but this information was not available for the studied test drinks. Implementation of a stomach volume compartment was not supported by the data given the current study design (i.e. focus on the effect of nutrients rather than volume).

The secretion of CCK was mediated through a signal from nutrients in duodenum (CCK_F) and upper jejunum (CCK_L) where the secreting cells are concentrated.[14] The use of precursor models where the release from the pool was mediated by a signal of the nutrients in the small intestine best predicted the two distinct peaks, characteristic of the postprandial release of CCK (*Figure 9, Figure 10*). This implementation was also used to mimic the exhaustion of the CCK secretory granules contained in the secretory cells.[15] Several CCK model parameters were estimated with a high uncertainty, likely due to the model complexity and to the lack of data. The reported parameters should therefore be interpreted with caution.

CCK is commonly described as the main factor involved in the postprandial gallbladder emptying.[15,97] Unexpectedly, while the postprandial CCK plasma

concentrations could to some extend be used to predict the gallbladder emptying, a lack of relationship with the nutritional content of the test drinks was observed. This could indicate the implication of other stimulatory factors of gallbladder emptying such as a combined hormonal and neural action.[15,97] Alternatively, when the postprandial gallbladder emptying was triggered by $efat_{duod}$, the resulting model had a simpler structure and improved predictive performances (*Figure 9*, *Figure 10*). In line with previous publications, carbohydrates had a relatively low potency (5.8%) to trigger the gallbladder emptying in comparison to proteins (87%) and fats (100%).[15,97]

The use of the TBA data were preferred over the use of the individual bile acids data. This approach avoided the need for the addition of conjugation and deconjugation processes into the model.[16,17] The determination of the structure and parameters of TBA distribution was supported by the use of radiolabeled total cholic acid data from the litterature.[50] The estimated volumes and clearance values were in line with the report of a rapid and contained distribution of TBA.[17,111] The total cholic acid and TBA were herein assumed to have very similar distribution, assumption which was supported by the work from Cowen *et al.* who showed that the protein binding and kinetic of disappearance were similar in most bile acids.[111] The postprandial TBA plasma concentrations were characterized by multiple peaks, which have been suggested to originate from the recirculation of reabsorbed bile acids.[22] However, assuming a constant gallbladder emptying did not allow the model to properly fit the data. Other have shown that postprandial gallbladder motility is characterized by sequences of emptying and refilling phases of variable intensities.[112,113] The hypothesis of a postprandial gallbladder refilling function was thus tested in the model and significantly improved the model predictions.

In addition to their effect on the gastric emptying rate and gallbladder emptying, some test drink properties were also associated with changes in the TBA EHC model parameters. Thus, the mean transit time of bile acids through the lower small intestine was found to be correlated to the amount of carbohydrates, an effect that has to our knowledge not been reported before. The fraction of TBA absorbed in the upper small intestine, was also significantly increased with the OGTT 75 g, possibly caused by a pH-related change of the ionized fraction of bile acids.[16,17] Finally, E_H was decreased with the high fat test drink, a finding that differs from reports by Angelin *et al.*[22] This effect could potentially be caused by the interaction of bile acids with the lipoproteins absorbed via the lymphatic system, thus possibly allowing them bypass the first-pass metabolism.[3,114]

This modeling framework has been developed using test drinks (i.e. liquid meals) data and extrapolation to solid meals has yet to be tested. Several additional assumptions such as the postprandial gallbladder refilling period had to be made. Despite these limitations the developed model should be considered as the first step towards more reliable predictions of the rate of gastric

emptying and of the postprandial TBA concentrations. Furthermore, this modeling framework could be used throughout drug development to predict the drug-drug interactions and food effects associated with gastric emptying[29,115], to link the postprandial changes in TBA plasma to changes in the drug absorption, or to support research on pathologies affecting the GI tract.

Treatment of Indian children with TB

The work from *Paper IV* describes how an NLME approach was used to establish the exposure-response of first line anti-TB therapy in children and to suggest dosing modifications.

In the first step, the PK of INH, RIF and PZA were characterized. For all three drugs, the relative bioavailability was found to be nonlinearly correlated to total body weight indicating reduced drug exposures in children with low body weight. The exposure to INH and RIF was also reduced in children with TB-HIV coinfection. Despite a contrasted effect of HIV in previous reports[61,71], HIV coinfection was herein associated with altered INH and RIF bioavailability and RIF clearance. The effects of body weight and HIV were likely the result of a complex combination of factors including: drug-drug interactions, formulations, age-related maturation, malabsorption, and malnutrition which were not independently distinguishable with the current study design.[116–118]

In the second step, the exposure-response relationship was established. *In vitro*, the activity of INH, RIF and PZA correlated well with both AUC and peak concentration.[119,120] To facilitate the translation between thrice-weekly and daily dosing in the model, AUC was retained as marker of drug exposure. The weekly RIF exposure at steady state was found to be the only independent predictor of treatment outcomes, which could be an indication that RIF was the most severely under-dosed anti-TB drug. In line with previous report, the body weight and TB-HIV coinfection had an impact on $P_{unfavorable}$ through their effect on the RIF exposure.[116,118,121–124] The established exposure-response relationship allowed the definition of a target weekly AUC for RIF based on actual pediatric data.

In the third step the exposure-response model was used to predict the treatment outcomes under different scenarios. The simulations exposed a clear trends toward higher $P_{unfavorable}$ under the previous thrice-weekly dosing as compared to the new once-daily dosing RNTCP recommendations.[63,65] $P_{unfavorable}$ was at the highest in the first weight band and in TB-HIV coinfected children, direct consequence of the decreased RIF exposure in these subgroups. This finding is in line with reports that higher RIF doses along with nutritional supplementation may significantly improve outcomes in TB-HIV coinfected children.[61,116,118,125,126]

This work represents a first step in the definition of a target exposure derived from actual pediatric data. Clinical practice in India is rapidly evolving and this work established a base to support the future revisions of pediatric dosing guidelines. More specifically, the model-based simulations suggested that higher anti-tuberculosis doses levels in children with low body weight or HIV coinfection, could potentially prevent treatment failure or death.

Conclusions

The work presented in this thesis improved the mechanical understanding of processes associated with the absorption of orally administered drugs. Specifically, this work identified and quantified the effect of influential factors of the erosion of HPMC matrix tablets, and established the relation between the nutritional intake, gastric emptying, gallbladder emptying and the EHC of bile acids. In addition, it highlighted the effect of impaired bioavailability on the occurrence of unfavorable treatment outcome in children with TB.

Specifically:

- An *in silico* erosion model for HPMC matrix tablets was developed using a simple set of *in vitro* dissolution profiles to predict the *in vivo* erosion. The presented methodology described how the *in vitro* effects of tablet formulations and experimental conditions were integrated into the *in silico* model to predict erosion time profiles of multiple HPMC matrix tablets under fasting and postprandial status. This study also exemplified how the *in silico* model could be used to inform decision-making through simulation of a typical tablet erosion profile and the extent of its variability.

- A model described the relationship between the caloric intake and the rate of gastric emptying. This model could play a crucial role in the prediction of drug-drug interactions and food effects associated with the rate of gastric emptying.

- The gastric emptying model was extended to predict the gallbladder emptying–refilling patterns and the EHC of TBA in response to various nutrients intake. This modeling framework could be used during the development of orally administered compounds by linking the absorption variability to postprandial changes in plasma bile acids concentrations.

- Low RIF exposures were linked to an increased $P_{unfavorable}$ in TB-infected underweight Indian children with or without concomitant HIV infection treated under a first line thrice weekly dosing regimen. RIF exposure was the lowest in children with low body weight or HIV coinfection. While the treatment outcome is expected to be improved under the new daily dosing regimen, the small children and/or with HIV coinfection are still

expected to display a poor treatment outcome and hence doses aiming to reduce the $P_{unfavorable}$ in these subjects have been suggested.

Acknowledgements

The work presented in this thesis was carried out at the *Department of Pharmaceutical Biosciences, Faculty of Pharmacy, Uppsala University*. This work would not have been possible without support from AstraZeneca and the Innovative Medicines Initiative Joint Undertaking (http://www.imi.europa.eu) under grant agreement number 115369, resources of which are composed of financial contribution from the European Union's Seventh Framework Programme (FP7/2007-2013) and EFPIA companies in kind contribution.

I am also grateful for the travel grants generously provided by the *Anna-Maria Lundin*'s foundation at *Smålands Nation* and *Apotekarsociteten* which allowed me to attend international conferences and trainings.

I would like to express my sincere gratitude to all who, in one way or another, have contributed to this thesis. Thanks to:

My supervisor *Prof. Mats Karlsson,* for welcoming me into your group and sharing your knowledge on Pharmacometrics with me. I have learned so much from you through these five years, but still not where you get all these incredible ideas. I am thankful that you let me go my own way even if this may have taken me away from my projects at times. I have always found it comforting to know that I could count on you through challenging times.

My co-supervisor *Dr. Martin Bergstrand*, one of the greatest supervisors I could hope for (by height and wisdom). You always took the time to explain the technical aspects of the projects and you taught me how to address real questions rather than "fitting the line through the dots". You welcomed me in Uppsala with a meal at Katalin, a bike and a roof, and I could never thank you enough for that.

All my co-authors, with special thanks to *Dr. Erik Söderlind*, *Sara Richardson* and *Alexandra Peric* for teaching me about *in vitro* dissolution testing and ER formulation design. *Dr. David Sonne*, *Dr. Morten Hansen* and *Prof. Filip Knop* for our great collaboration on gastric emptying and bile acids papers. *Dr. Radojka Savic*, *Dr. Kelly Dooley,* and *Dr. Geetha Ramachandran* for teaching me about anti-TB treatment in pediatrics. *Rada,* I also want to thank you for welcoming me in your group at *UCSF.*

All my colleagues in the *Orbito* consortium, with a special thanks *Dr. Mirko Koziolek*, *Michael Grimm* and *Prof. Werner Weitschies* for welcoming me in your group at Greifswald and to *Dr. Xavier Pepin*, *Dr. Adam Darwich*, *Prof. Leon Aarons*, *Prof. Amin Rostami-Hochaghan, Dr. Massoud Jamei,* and *Dr. David Turner* for our interactions through my projects and the different work packages.

To colleagues at *Pharmetheus* and especially to *Dr. Marie Sandström* for always making me feel welcome, and to *Dr. Joakim Nyberg*, *Dr. Jackob Ribbing*, *Dr. Mats Magnusson*, *Dr. Niclas Jonsson* and *Arnaud Pharasyn* for teaching me so much.

My half-time opponents *Dr. Maria Kjellson*, *Dr. Klas Petersson,* and *Dr. Erik Sjögren* for the nice discussion and for giving me valuable feedback on my thesis.

Prof. Margareta Hammarlund-Udenaes, *Prof. Lena Friberg*, *Prof. Ulrika Simonsson*, *Dr. Andrew Hooker*, *Dr. Siv Jönsson*, *Dr. Elisabet Nielsen*, *Dr. Kristin Karlsson, and Dr. Irena Loryan* for creating such a great working environment, bringing a variety of knowledge and opinions.

Magnus, *Tobias* and *Jerker* for IT support, *Jörgen* for giving us the chance to teach, *Marina*, *Elisabeth*, *Ulrica* and *Karin* for administrative help, and *Agneta* for your help in the department. *Kajsa*, *Rikard*, and *Svetlana* for your great work on PsN and always keeping your door open for questions.

All contributors to the xpose project: *Andy*, *Sebastian U*, *Anna O*, *Elodie*, *Mike*, *Kajsa*, *Ron* and *Mats*.

The visiting students *Rasmus*, *Stein*, *Dirk Jan*, *Gulbeyaz*, *Marjiam*, *Elham* and *Tore* for sharing your experience with us.

My office mates *Jesmin* for bringing good vibes in that freezing room, *Nebojsa* for telling me about the true meaning of love, *Ari* for our bike talks, *Ida* for putting money into that jar, too bad we could not get you to fill it up, *Siti* for not spying on us (who were you working for?), *Waqas* for your positive attitude, *Brendan* for eh … ursäkta, *Gunnar* for raising the awareness in me, we have way too many interesting things to talk about and I hope that we will continue to do so in a cryptographic manner.

All colleagues, past and present, *Julia* for sharing your personnummer stories with me, *Philippe* for helping me out with PBPK, *Sebastian W* for our shiny discussions, *Eva* for your work tips, *Yasunori* for attempting to make D&D casual, *Anna L* for teaching us the Italian way, *Chayan, Lani* and *Gopi* for the

amazing cuisine, but yes it was spicy, *Margreke* and *Elke* for the Dutch laughs, *Camille, Lenaïg* and *Estelle* for maintaining the French presence in the group, *Ronald* for taking me back home, *Steve* for *vires in numeris*, *Chenyan* for taking over the PM wiki, *Marina* for the discussions on covariate selection, *Henrik* for teaching us about saddle reset, although every time you say "saddle" I picture you on that tiny horse, *Gustaf* for doing that diabetic project with me, *Moustafa* for trying to convince me that the Weibull model is the solution to everything, *Sofia* for the baby tips, *Erik M* for your help on HPLC assays, *Xiaomei* for coming back, *Yevgen* for our R/math talks, *Anders K* for the botanical classes, *Anders T* for the nice talks on TV shows, *Robin* for your help on RIF, *João* for your secret CPT recipe, *Elin* for your incredible dedication to make the world a better place, *Thomas* for your wisdom, *Paolo* for your tips on the TB project and for the stories of your bike, *David* and *Salim* for being the best gym buddies, *Aziz* for our movie discussions and for your acting tips, *Anne-Gaëlle* and *Ana* for the good times at work and after-work. But also, to *Annika*, *Åsa* for showing us la vie en ~~rose~~ violet*, Eric S* for keeping your cool when your computer crashed, *Victor* for disclosing your results after all, *Oskar A* for our talks on paracetamol, *Oskar C* for our talks on TB, *Shijun*, *Sreenath, Chenhui, Chunli, Winn*, and *Yang* for the sweets you always brought from your trips.

A *Marie-Paule* pour partager ma passion pour les randonnées gastronomiques et pour m'avoir accueilli chez vous à bras ouverts.

A mes parents et *Guillaume* pour m'avoir supporté dans mes projets malgré le fait que j'ai souvent été loin de vous.

A *Emilie*, tu as changé ma vie, c'est en partie grâce à ton amour, ta force et ton soutien que j'ai pu accomplir tout ce travail. Je te dois tellement ! Je suis impatient de commencer le prochain chapitre de nos aventures.

A ma petite *Alice*, merci d'avoir apporté tant de bonheur dans notre famille, tu nous as rejoint il n'y a pas si longtemps et pourtant tu déjà changé nos vies, et te voir grandir est tellement gratifiant !

Benjamin G.

References

1. Sjögren, E. *et al.* In vivo methods for drug absorption – Comparative physiologies, model selection, correlations with in vitro methods (IVIVC), and applications for formulation/API/excipient characterization including food effects. *Eur. J. Pharm. Sci.* **57**, 99–151 (2014).
2. Amidon, G. L., Lennernäs, H., Shah, V. P. & Crison, J. R. A theoretical basis for a biopharmaceutic drug classification: The correlation of in vitro drug product dissolution and in vivo bioavailability. *Pharm. Res. An Off. J. Am. Assoc. Pharm. Sci.* **12**, 413–420 (1995).
3. Charman, W. N., Porter, C. J., Mithani, S. & Dressman, J. B. Physicochemical and physiological mechanisms for the effects of food on drug absorption : The role of lipids and pH. *J. Pharm. Sci.* **86**, 269–282 (1997).
4. Swaminathan, S. & Ramachandran, G. Challenges in childhood tuberculosis. *Clin. Pharmacol. Ther.* **98**, 240–244 (2015).
5. Lennernäs, H. *et al.* Regional Jejunal Perfusion, a New in Vivo Approach to Study Oral Drug Absorption in Man. *Pharm. Res. An Off. J. Am. Assoc. Pharm. Sci.* **9**, 1243–1251 (1992).
6. Jantratid, E., Janssen, N., Reppas, C. & Dressman, J. B. Dissolution media simulating conditions in the proximal human gastrointestinal tract: an update. *Pharm. Res.* **25**, 1663–76 (2008).
7. Mould, D. R. & Upton, R. N. Basic Concepts in Population Modeling, Simulation, and Model-Based Drug Development. *CPT Pharmacometrics Syst. Pharmacol.* **1**, e6 (2012).
8. Bergstrand, M., Söderlind, E., Eriksson, U. G., Weitschies, W. & Karlsson, M. O. A semi-mechanistic modeling strategy to link in vitro and in vivo drug release for modified release formulations. *Pharm. Res.* **29**, 695–706 (2012).
9. Hénin, E., Bergstrand, M., Weitschies, W. & Karlsson, M. O. Meta-analysis of magnetic marker monitoring data to characterize the movement of single unit dosage forms though the gastrointestinal tract under fed and fasting conditions. *Pharm. Res.* **33**, 751–762 (2016).
10. Pharmacokinetics, P. Guidance for Industry Guidance for Industry Population Pharmacokinetics. 20852–1448 (1999).
11. Camilleri, M. Integrated upper gastrointestinal response to food intake. *Gastroenterology* **131**, 640–58 (2006).
12. Deloose, E., Janssen, P., Depoortere, I. & Tack, J. The migrating motor complex: control mechanisms and its role in health and disease. *Nat. Rev. Gastroenterol. Hepatol.* **9**, 271–85 (2012).
13. Moran, T. H., Wirth, J. B., Schwartz, G. J. & McHugh, P. R. Interactions

between gastric volume and duodenal nutrients in the control of liquid gastric emptying. *Am. J. Physiol.* **276**, R997–R1002 (1999).
14. Agersnap, M. & Rehfeld, J. F. Nonsulfated cholecystokinins in the small intestine of pigs and rats. *Peptides* **71**, 121–7 (2015).
15. Liddle, R. A. Cholecystokinin cells. *Annu. Rev. Physiol.* **59**, 221–242 (1997).
16. Stamp, D. & Jenkins, G. An Overview of Bile-Acid Synthesis, Chemistry and Function. In *Bile Acids Toxicol. Bioactivity* (Jenkins, G. & Hardie, L. J.) 1–13 (Royal Society of Chemistry, 2008).doi:10.1039/9781847558336-00001
17. Hofmann, A. F. Enterohepatic circulation of bile acids. *Handb. Physiol. - Gastrointest. Syst.* **19**, 567–596 (1978).
18. Behar, J. Physiology and Pathophysiology of the Biliary Tract: The Gallbladder and Sphincter of Oddi—A Review. *ISRN Physiol.* **2013**, 1–15 (2013).
19. Angelin, B., Einarsson, K. & Hellström, K. Evidence for the absorption of bile acids in the proximal small intestine of normo- and hyperlipidaemic subjects. *Gut* **17**, 420–5 (1976).
20. Angelin, B. & Björkhem, I. Postprandial serum bile acids in healthy man. Evidence for differences in absorptive pattern between individual bile acids. *Gut* **18**, 606 (1977).
21. Roberts, M. S., Magnusson, B. M., Burczynski, F. J. & Weiss, M. Enterohepatic circulation: physiological, pharmacokinetic and clinical implications. *Clin. Pharmacokinet.* **41**, 751–790 (2002).
22. Angelin, B., Björkhem, I., Einarsson, K. & Ewerth, S. Hepatic Uptake of Bile Acids in Man. *J. Clin. Invest.* **70**, 724–731 (1982).
23. Convention, U. S. P. *The United States Pharmacopeia . Steriliz. Steril. Assur. Compend. Artic. Good Manuf. Pract.* **US 23rd**, (1995).
24. Committee for Medicinal Products for Human Use (CHMP) Guideline on the pharmacokinetic and clinical evaluation of modified release dosage forms. *EMA* (2014).
25. FDA Guidance for Industry Extended Release Oral Dosage Forms: Development, Evaluation, and Application of In Vitro/In Vivo Correlations U.S. *Evaluation* (1997).
26. Mitra, A., Kesisoglou, F. & Dogterom, P. Application of absorption modeling to predict bioequivalence outcome of two batches of etoricoxib tablets. *AAPS PharmSciTech* **16**, 76–84 (2015).
27. Wu, C. Y. & Benet, L. Z. Predicting drug disposition via application of BCS: Transport/absorption/ elimination interplay and development of a biopharmaceutics drug disposition classification system. *Pharm. Res.* **22**, 11–23 (2005).
28. Vieth, M. *et al.* Characteristic Physical Properties and Structural Fragments of Marketed Oral Drugs. *J. Med. Chem.* **47**, 224–232 (2004).
29. Fleisher, D., Li, C., Zhou, Y., Pao, L. H. & Karim, A. Drug, meal and formulation interactions influencing drug absorption after oral administration. Clinical implications. *Clin. Pharmacokinet.* **36**, 233–254 (1999).

30. Wiedmann, T. S. & Kamel, L. Examination of the solubilization of drugs by bile salt micelles. *J. Pharm. Sci.* **91**, 1743–1764 (2002).
31. Kostewicz, E. S. *et al.* PBPK models for the prediction of in vivo performance of oral dosage forms. *Eur. J. Pharm. Sci.* **57**, 300–21 (2014).
32. Becker, C. *et al.* Biowaiver monographs for immediate release solid oral dosage forms: Isoniazid. *J. Pharm. Sci.* **96**, 522–531 (2007).
33. Becker, C. *et al.* Biowaiver monographs for immediate release solid oral dosage forms: Rifampicin. *J. Pharm. Sci.* **98**, 2252–2267 (2009).
34. Kalantzi, L. *et al.* Biowaiver monographs for immediate release solid oral dosage forms: Acetaminophen (Paracetamol). *J. Pharm. Sci.* **95**, 4–14 (2006).
35. Becker, C. *et al.* Biowaiver monographs for immediate release solid oral dosage forms: Pyrazinamide. *J. Pharm. Sci.* **97**, 3709–3720 (2008).
36. Shargel, L., Yu, A. B. C. & Wu-Pong, S. Modified-Release Drug Products. In *Appl. Biopharm. Pharmacokinet.* 469 (2012).
37. Tajarobi, F., Abrahmsén-Alami, S., Hansen, M. & Larsson, A. The impact of dose and solubility of additives on the release from HPMC matrix tablets-identifying critical conditions. *Pharm. Res.* **26**, 1496–1503 (2009).
38. Viridén, A., Abrahmsén-Alami, S., Wittgren, B. & Larsson, A. Release of theophylline and carbamazepine from matrix tablets - Consequences of HPMC chemical heterogeneity. *Eur. J. Pharm. Biopharm.* **78**, 470–479 (2011).
39. Maderuelo, C., Zarzuelo, A. & Lanao, J. M. Critical factors in the release of drugs from sustained release hydrophilic matrices. *J. Control. Release* **154**, 2–19 (2011).
40. Gajdošová, M., Pěček, D., Sarvašová, N., Grof, Z. & Štěpánek, F. Effect of hydrophobic inclusions on polymer swelling kinetics studied by magnetic resonance imaging. *Int. J. Pharm.* **500**, 136–143 (2016).
41. Viridén, A., Wittgren, B., Andersson, T. & Larsson, A. The effect of chemical heterogeneity of HPMC on polymer release from matrix tablets. *Eur. J. Pharm. Sci.* **36**, 392–400 (2009).
42. McAllister, M. Dynamic dissolution: A step closer to predictive dissolution testing? *Mol. Pharm.* **7**, 1374–1387 (2010).
43. Kostewicz, E. S. *et al.* In vitro models for the prediction of in vivo performance of oral dosage forms. *Eur. J. Pharm. Sci.* **57**, 342–366 (2014).
44. Guerra, A. *et al.* Relevance and challenges in modeling human gastric and small intestinal digestion. *Trends Biotechnol.* **30**, 591–600 (2012).
45. Weitschies, W., Blume, H. & Mönnikes, H. Magnetic marker monitoring: High resolution real-time tracking of oral solid dosage forms in the gastrointestinal tract. *Eur. J. Pharm. Biopharm.* **74**, 93–101 (2010).
46. Weitschies, W. & Wilson, C. G. In vivo imaging of drug delivery systems in the gastrointestinal tract. *Int. J. Pharm.* **417**, 216–226 (2011).
47. Clements, J. A., Heading, R. C., Nimmo, W. S. & Prescott, L. F. Kinetics of acetaminophen absorption and gastric emptying in man. *Clin. Pharmacol. Ther.* **24**, 420–31 (1978).

48. Willems, M., Otto Quartero, A. & Numans, M. E. How useful is paracetamol absorption as a marker of gastric emptying? A systematic literature study. *Dig. Dis. Sci.* **46**, 2256–2262 (2001).
49. Raffa, R. B., Pergolizzi, J. V, Taylor, R., Decker, J. F. & Patrick, J. T. Acetaminophen (paracetamol) oral absorption and clinical influences. *Pain Pract.* **14**, 668–77 (2014).
50. Engelking, L. R., Barnes, S. & Dasher, C. A. Radiolabeled bile acid clearance in control subjects and patients with liver disease. *Clin. Sci.* **57**, 499–508 (1979).
51. World Health Organization Tuberculosis Fact sheet N°104. *Media Cent. Tuberc.* (2018).
52. WHO *Global tuberculosis report 2017*. *World Heal. Organ. Press* (2017).doi:ISBN 978 92 4 156539 4
53. Ramachandran, G., Kumar, A. K. H. & Swaminathan, S. Pharmacokinetics of anti-tuberculosis drugs in children. *Indian J. Pediatr.* **78**, 435–442 (2011).
54. Pai, M., Daftary, A. & Satyanarayana, S. TB control: challenges and opportunities for India. *Trans. R. Soc. Trop. Med. Hyg.* **110**, 158–160 (2015).
55. Mukherjee, A. *et al.* Pharmacokinetics of isoniazid, rifampicin, pyrazinamide and ethambutol in Indian children. *BMC Infect. Dis.* **15**, 126 (2015).
56. Ramachandran, G. *et al.* Pharmacokinetics of first-line antituberculosis drugs in HIV-infected children with tuberculosis treated with intermittent regimens in India. *Antimicrob. Agents Chemother.* **59**, 1162–1167 (2015).
57. Ramachandran, G. *et al.* Age, nutritional status and INH acetylator status affect pharmacokinetics of anti-tuberculosis drugs in children. *Int. J. Tuberc. Lung Dis.* **17**, 800–806 (2013).
58. Swaminathan, S. *et al.* Drug concentration thresholds predictive of therapy failure and death in children with tuberculosis: Bread crumb trails in random forests. *Clin. Infect. Dis.* **63**, S63–S74 (2016).
59. Schaaf, H. S., Garcia-Prats, A. J. & Donald, P. R. Antituberculosis drugs in children. *Clin. Pharmacol. Ther.* **98**, 252–265 (2015).
60. Verma, R., Khanna, P. & Mehta, B. Revised national tuberculosis control program in India: the need to strengthen. *Int. J. Prev. Med.* **4**, 1–5 (2013).
61. Ramachandran, G. *et al.* Low serum concentrations of rifampicin and pyrazinamide associated with poor treatment outcomes in children with tuberculosis related to HIV status. *Pediatr. Infect. Dis. J.* **35**, 1 (2016).
62. Hemanth Kumar, A. K. *et al.* Pharmacokinetics of thrice-weekly rifampicin, isoniazid and pyrazinamide in adult tuberculosis patients in India. *Int. J. Tuberc. Lung Dis.* **20**, 1236–1241 (2016).
63. National guidelines on diagnosis and treatment of pediatric tuberculosis. Central TB division, Government of India. (2012).
64. World Health Organization (WHO) Guidance for national tuberculosis programmes on the management of tuberculosis in children - 2nd ed. *Geneva Contract No. WHO/HTM/TB/2014.03* (2014).doi:10.1007/s007690000247

65. Central TB division. Technical and operational guidelines for tuberculosis control in India 2016: Revised national TB control programme. New Delhi: Ministry of health and family welfare. (2016).
66. IANS Government rolls out daily drug regimen for TB. *Bus. Stand.* (2017).at <http://www.business-standard.com/article/news-ians/government-rolls-out-daily-drug-regimen-for-tb-117111700772_1.html>
67. DiMasi, J. A., Grabowski, H. G. & Hansen, R. W. Innovation in the pharmaceutical industry: New estimates of R&D costs. *J. Health Econ.* **47**, 20–33 (2016).
68. U.S. Food and Drug Administration *Challenge and Opportunity on the Critical Path to New Medical Products*. *Rev. Lit. Arts Am.* (2004).
69. Ette, E. I. & Williams, P. J. *Pharmacometrics: The Science of Quantitative Pharmacology*. *Pharmacometrics Sci. Quant. Pharmacol.* (2006).doi:10.1002/9780470087978
70. FDA Pharmacometrics at FDA. at <https://www.fda.gov/AboutFDA/CentersOffices/OfficeofMedicalProductsandTobacco/CDER/ucm167032.htm>
71. Zvada, S. P. *et al.* Population pharmacokinetics of rifampicin, pyrazinamide and isoniazid in children with tuberculosis: In silico evaluation of currently recommended doses. *J. Antimicrob. Chemother.* **69**, 1339–1349 (2014).
72. Gisleskog, P. O., Karlsson, M. O. & Beal, S. L. Use of prior information to stabilize a population data analysis. *J. Pharmacokinet. Pharmacodyn.* **29**, 473–505 (2002).
73. Tsamandouras, N., Rostami-Hodjegan, A. & Aarons, L. Combining the "bottom up" and "top down" approaches in pharmacokinetic modelling: Fitting PBPK models to observed clinical data. *Br. J. Clin. Pharmacol.* **79**, 48–55 (2015).
74. Jones, H. M. *et al.* Simulation of human intravenous and oral pharmacokinetics of 21 diverse compounds using physiologically based pharmacokinetic modelling. *Clin. Pharmacokinet.* **50**, 331–347 (2011).
75. Agoram, B., Woltosz, W. S. & Bolger, M. B. Predicting the impact of physiological and biochemical processes on oral drug bioavailability. *Adv. Drug Deliv. Rev.* **50 Suppl 1**, S41–S67 (2001).
76. Jamei, M. *et al.* Population-based mechanistic prediction of oral drug absorption. *AAPS J.* **11**, 225–237 (2009).
77. Keizer, R. J., Karlsson, M. O. & Hooker, A. Modeling and simulation workbench for NONMEM: Tutorial on Pirana, PsN, and Xpose. *CPT pharmacometrics Syst. Pharmacol.* **2**, e50 (2013).
78. Guiastrennec, B. *et al.* xpose: Diagnostics for Pharmacometric Models. (2018).
79. Bergstrand, M., Hooker, A. C., Wallin, J. E. & Karlsson, M. O. Prediction-corrected visual predictive checks for diagnosing nonlinear mixed-effects models. *AAPS J.* **13**, 143–151 (2011).
80. Petersson, K. J. F., Hanze, E., Savic, R. M. & Karlsson, M. O. Semiparametric distributions with estimated shape parameters. *Pharm. Res.* **26**, 2174–2185 (2009).

81. Anderson, B. J. & Holford, N. H. G. Mechanistic basis of using body size and maturation to predict clearance in humans. *Drug Metab. Pharmacokinet.* **24**, 25–36 (2009).
82. Jain, A. K. *et al.* The influence of hydroxypropyl methylcellulose (HPMC) molecular weight, concentration and effect of food on in vivo erosion behavior of HPMC matrix tablets. *J. Control. Release* **187**, 50–58 (2014).
83. Ghimire, M. *et al.* In-vitro and in-vivo erosion profiles of hydroxypropylmethylcellulose (HPMC) matrix tablets. *J. Control. Release* **147**, 70–75 (2010).
84. Dressman, J. B. *et al.* Upper gastrointestinal (GI) pH in young, healthy men and women. *Pharm. Res.* **7**, 756–761 (1990).
85. Evans, D. F. *et al.* Measurement of gastrointestinal pH profiles in normal ambulant human subjects. *Gut* **29**, 1035–41 (1988).
86. Merrill, A. L. & Watt, B. K. Energy values of food: basis and derivation. *Agric. Handboook* **74**, 1–105 (1973).
87. Alskär, O. *et al.* Semimechanistic model describing gastric emptying and glucose absorption in healthy subjects and patients with type 2 diabetes. *J. Clin. Pharmacol.* **56**, 340–348 (2016).
88. Ogungbenro, K. *et al.* A semi-mechanistic gastric emptying model for the population pharmacokinetic analysis of orally administered acetaminophen in critically ill patients. *Pharm. Res.* **28**, 394–404 (2011).
89. Zuppa, A. F. *et al.* Safety and population pharmacokinetic analysis of intravenous acetaminophen in neonates, infants, children, and adolescents with pain or Fever. *J. Pediatr. Pharmacol. Ther.* **16**, 246–61 (2011).
90. Hunt, J. N. & Stubbs, D. F. The volume and energy content of meals as determinants of gastric emptying. *J. Physiol.* **245**, 209–225 (1975).
91. Hénin, E., Bergstrand, M., Standing, J. F. & Karlsson, M. O. A mechanism-based approach for absorption modeling: the gastro-intestinal transit time (GITT) model. *AAPS J.* **14**, 155–63 (2012).
92. Sonne, D. P., Rehfeld, J. F., Holst, J. J., Vilsboll, T. & Knop, F. K. Postprandial gallbladder emptying in patients with type 2 diabetes: potential implications for bile-induced secretion of glucagon-like peptide 1. *Eur. J. Endocrinol.* **171**, 407–419 (2014).
93. Sonne, D. P. *et al.* Postprandial gut hormone responses and glucose metabolism in cholecystectomized patients. *AJP Gastrointest. Liver Physiol.* **304**, 413–419 (2013).
94. Sharma, A., Ebling, W. F. & Jusko, W. J. Precursor-dependent indirect pharmacodynamic response model for tolerance and rebound phenomena. *J. Pharm. Sci.* **87**, 1577–84 (1998).
95. Hopman, W. P., Jansen, J. B. & Lamers, C. B. Comparative study of the effects of equal amounts of fat, protein, and starch on plasma cholecystokinin in man. *Scand. J. Gastroenterol.* **20**, 843–7 (1985).
96. Small, B. G., Wendt, B., Jamei, M. & Johnson, T. N. Prediction of liver volume – a population-based approach to meta-analysis of paediatric, adult and geriatric populations – an update. *Biopharm. Drug Dispos.* **38**, 290–300 (2017).

97. Froehlich, F., Gonvers, J. J. & Fried, M. Role of nutrient fat and cholecystokinin in regulation of gallbladder emptying in man. *Dig Dis Sci* **40**, 529–533 (1995).
98. Matyja, A. *et al.* Telocytes: New insight into the pathogenesis of gallstone disease. *J. Cell. Mol. Med.* **17**, 734–742 (2013).
99. Yang, J., Jamei, M., Yeo, K. R., Rostami-Hodjegan, A. & Tucker, G. T. Misuse of the well-stirred model of hepatic drug clearance. *Drug Metab. Dispos.* **35**, 501–502 (2007).
100. Chirehwa, M. T. *et al.* Model-based evaluation of higher doses of rifampin using a semimechanistic model incorporating autoinduction and saturation of hepatic extraction. *Antimicrob. Agents Chemother.* **60**, 487–494 (2016).
101. Savic, R. M., Jonker, D. M., Kerbusch, T. & Karlsson, M. O. Implementation of a transit compartment model for describing drug absorption in pharmacokinetic studies. *J. Pharmacokinet. Pharmacodyn.* **34**, 711–726 (2007).
102. Ellard, G. a & Gammon, P. T. Pharmacokinetics of isoniazid metabolism in man. *J. Pharmacokinet. Biopharm.* **4**, 83–113 (1976).
103. World Health Organization (WHO) Target Regimen Profiles for TB Treatment. *Geneva Contract No. WHO/HTM/TB/2016.16* (2016).
104. Tajarobi, F., Abrahmsén-Alami, S., Carlsson, A. S. & Larsson, A. Simultaneous probing of swelling, erosion and dissolution by NMR-microimaging-Effect of solubility of additives on HPMC matrix tablets. *Eur. J. Pharm. Sci.* **37**, 89–97 (2009).
105. Asare-Addo, K. *et al.* The effect of pH and ionic strength of dissolution media on in-vitro release of two model drugs of different solubilities from HPMC matrices. *Colloids Surfaces B Biointerfaces* **111**, 384–391 (2013).
106. Bajwa, G. S., Hoebler, K., Sammon, C., Timmins, P. & Melia, C. D. Microstructural imaging of early gel layer formation in HPMC matrices. *J. Pharm. Sci.* **95**, 2145–2157 (2006).
107. Mitchell, K. *et al.* The influence of additives on the cloud point, disintegration and dissolution of hydroxypropylmethylcellulose gels and matrix tablets. *Int. J. Pharm.* **66**, 233–242 (1990).
108. Bergstrand, M., Söderlind, E., Eriksson, U. G., Weitschies, W. & Karlsson, M. O. A semi-mechanistic modeling strategy for characterization of regional absorption properties and prospective prediction of plasma concentrations following administration of new modified release formulations. *Pharm. Res.* **29**, 574–584 (2012).
109. Siegel, J. A. *et al.* Biphasic nature of gastric emptying. *Gut* **29**, 85–9 (1988).
110. Calbet, J. & MacLean, D. Role of caloric content on gastric emptying in humans. *J. Physiol.* **498**, 553–559 (1997).
111. Cowen, A. E., Korman, M. G., Hofmann, A. F. & Thomas, P. J. Plasma disappearance of radioactivity after intravenous injection of labeled bile acids in man. *Gastroenterology* **68**, 1567–1573 (1975).
112. Howard, P. J., Murphy, G. M. & Dowling, R. H. Gall bladder emptying patterns in response to a normal meal in healthy subjects and patients with gall stones: ultrasound study. *Gut* **32**, 1406–1411 (1991).

113. Jazrawi, R. P. *et al.* Postprandial gallbladder motor function: Refilling and turnover of bile in health and in cholelithiasis. *Gastroenterology* **109**, 582–591 (1995).
114. Salvioli, G., Lugli, R., Pradelli, J. M. & Gigliotti, G. Bile acid binding in plasma: the importance of lipoproteins. *FEBS Lett.* **187**, 272–276 (1985).
115. Greiff, J. M. C. & Rowbotham, D. Pharmacokinetic Drug Interactions with Gastrointestinal Motility Modifying Agents. *Clin. Pharmacokinet.* **27**, 447–461 (1994).
116. Gurumurthy, P. *et al.* Decreased bioavailability of rifampin and other antituberculosis drugs in patients with advanced human immunodeficiency virus disease. *Society* **48**, 4473–4475 (2004).
117. Graham, S. M. *et al.* Low levels of pyrazinamide and ethambutol in children with tuberculosis and impact of age, nutritional status, and human immunodeficiency virus infection. *Society* **50**, 407–413 (2006).
118. Bekker, A. *et al.* Ethambutol in infants dosed according to revised WHO-recommended treatment guidelines. **60**, 2171–2179 (2016).
119. Jayaram, R. *et al.* Pharmacokinetics-pharmacodynamics of rifampin in an aerosol infection model of tuberculosis. *Antimicrob.Agents Chemother.* **47**, 2118–2124 (2003).
120. Gumbo, T., Pasipanodya, J. G., Nuermberger, E., Romero, K. & Hanna, D. Correlations between the hollow fiber model of tuberculosis and therapeutic events in tuberculosis patients: Learn and confirm. *Clin. Infect. Dis.* **61**, S18–S24 (2015).
121. Munoz-Sellart, M., Yassin, M. A., Tumato, M., Merid, Y. & Cuevas, L. E. Treatment outcome in children with tuberculosis in southern Ethiopia. *Scand J Infect Dis* **41**, 450–455 (2009).
122. Hailu, D., Abegaz, W. E. & Belay, M. Childhood tuberculosis and its treatment outcomes in Addis Ababa: a 5-years retrospective study. *BMC Pediatr.* **14**, 61 (2014).
123. Mcilleron, H. *et al.* Reduced antituberculosis drug concentrations in HIV-infected patients who are men or have low weight : Implications for international dosing guidelines. **56**, 3232–3238 (2012).
124. Antwi, S. *et al.* Pharmacokinetics of the first-line antituberculosis drugs in Ghanaian children with tuberculosis with or without HIV coinfection. *Antimicrob. Agents Chemother.* **61**, (2017).
125. Jeremiah, K. *et al.* Nutritional supplementation increases rifampin exposure among tuberculosis patients coinfected with HIV. *Antimicrob. Agents Chemother.* **58**, 3468–3474 (2014).
126. Merle, C. S. *et al.* High-dose rifampicin tuberculosis treatment regimen to reduce 12-month mortality of TB/HIV co-infected patients: The RAFA trial results. *21st Int. AIDS Conf.* **WEAB0205LB**, (2017).

Acta Universitatis Upsaliensis

Digital Comprehensive Summaries of Uppsala Dissertations from the Faculty of Pharmacy 246

Editor: The Dean of the Faculty of Pharmacy

A doctoral dissertation from the Faculty of Pharmacy, Uppsala University, is usually a summary of a number of papers. A few copies of the complete dissertation are kept at major Swedish research libraries, while the summary alone is distributed internationally through the series Digital Comprehensive Summaries of Uppsala Dissertations from the Faculty of Pharmacy. (Prior to January, 2005, the series was published under the title "Comprehensive Summaries of Uppsala Dissertations from the Faculty of Pharmacy".)

Distribution: publications.uu.se
urn:nbn:se:uu:diva-340238

ACTA
UNIVERSITATIS
UPSALIENSIS
UPPSALA
2018